Mechanical Properties and Constitutive Modelling of UHPC with Ultra Fine Waste Glass Powder (UFWGP), Micro Silica, Fly Ash and Steel and Polypropylene Fibres

Ayesha Ayub[1], Asad-ur-Rehman Khan[2,*] and Shamsoon Fareed[2]

[1] Department of Urban & Infrastructure Engineering, NED University of Engineering & Technology, Karachi, Pakistan

[2] Department of Civil Engineering, NED University of Engineering & Technology, Karachi, Pakistan

INFORMATION

Keywords:
Ultra-high-performance concrete
mechanical properties
constitutive modelling
stress-strain curves
fibres

DOI: 10.23967/j.rimni.2026.10.77623

SCIPEDIA
Revista Internacional de Métodos Numéricos para Cálculo y Diseño en Ingeniería
Revista Internacional Métodos numéricos para cálculo y diseño en ingeniería
RIMNI
In cooperation with CIMNE

Mechanical Properties and Constitutive Modelling of UHPC with Ultra Fine Waste Glass Powder (UFWGP), Micro Silica, Fly Ash and Steel and Polypropylene Fibres

Ayesha Ayub[1], **Asad-ur-Rehman Khan**[2,*] **and Shamsoon Fareed**[2]

[1]Department of Urban & Infrastructure Engineering, NED University of Engineering & Technology, Karachi, Pakistan

[2]Department of Civil Engineering, NED University of Engineering & Technology, Karachi, Pakistan

ABSTRACT

Ultra-high-performance concrete (UHPC) offers superior mechanical performance but remains limited by high cement content, sustainability concerns, and the lack of reliable constitutive models capable of capturing its full stress–strain response including pre-peak and post-peak behaviour. This study presents an integrated experimental and constitutive modelling investigation of UHPC incorporating ultra-fine waste glass powder, micro silica, fly ash, and different fibre reinforcement. Two UHPC mix designs with a water-to-cementitious material ratio of 0.20 were developed, yielding 24 independent mixtures. Cement was partially replaced with 20% ultra-fine waste glass powder and combined with either micro silica or fly ash. Fibre reinforcement was introduced independently using 2% straight steel fibres and 1.5% crimped polypropylene fibres to evaluate flowability, viscosity, uniaxial compressive strength, modulus of elasticity, splitting tensile strength, flexural strength and drying shrinkage behaviour. Experimental results demonstrate that UHPC with micro silica, UFWGP and steel fibres, prepared following the ACI 239 R-18 mix design, achieved the highest 28 days compressive, splitting tensile and flexural strength of 144.8, 12.8 and 36.1 MPa, respectively. Steel fibre-reinforced mixes exhibited up to a 42% increase in compressive strength and significantly enhanced post-peak ductility compared to the control mix (without fibre). Crimped Polypropylene fibre-reinforced UHPC attained compressive strength up to 129.7 MPa, provided improved strain capacity, and effectively reduced drying shrinkage, highlighting their suitability for crack control and deformation mitigation. The incorporation of UFWGP consistently improved flowability, reduced viscosity, and enhanced mechanical performance, while fly ash improved rheological behaviour but resulted in lower early-age strength compared to micro silica-based mixes. To capture the compressive response of UHPC, an elasto-damage model previously proposed by Khan and Zahra was reformulated by recalibrating the compression damage parameter (β) using experimentally derived and literature based compressive strength and elastic modulus. The proposed model reproduces both pre-peak and post-peak stress–strain behaviour, with prediction errors generally within $\pm 7\%$ of experimental results ranging from 72.4 to 148.5 MPa. The findings provide robust experimental evidence and a validated constitutive framework for the sustainable design and structural application of UHPC.

OPEN ACCESS

Received: 13/12/2025

Accepted: 19/01/2026

DOI
10.23967/j.rimni.2026.10.77623

Keywords:
Ultra-high-performance concrete
mechanical properties
constitutive modelling
stress-strain curves
fibres

*Correspondence: Asad-ur-Rehman Khan (asadkhan@neduet.edu.pk).

1 Introduction

Ultra-high-performance concrete (UHPC) is a modern concrete with exceptional performance, including enhanced mechanical characteristics with ultra-high compressive strength (>120 MPa), improved ductility, and superior durability [1]. Despite these advantages, UHPC remains limited by high cement content, significant environmental burden, and heavy dependency on silica fume and steel fibres, creating a need for more sustainable binder systems, alternative fibre types, and standardized tools for evaluating binder system and fibres efficiency [2]. Additionally, accurately predicting the mechanical behavior of UHPC requires robust constitutive models that can capture the effects of fibre reinforcement, binder composition, and full stress–strain response including pre and post-peak behaviour, which are critical for safe structural design and numerical simulations.

Although UHPC exhibits complex mechanical behavior, many experimental studies primarily focus on compressive strength and compressive stress–strain response. This emphasis arises because key parameters used in constitutive modeling such as peak compressive stress, peak strain, elastic modulus, and damage evolution are predominantly derived from compressive behavior. Consequently, accurate characterization of compressive strength is essential for reliable calibration and application of constitutive models in numerical simulations and structural design, explaining the primary focus on compression in UHPC investigation. Traditionally, in UHPC mix design, micro silica (MS or silica fume) along with Ordinary Portland Cement (OPC) is used as a binder. Its ultrafine particle size and pore-filling capacity contribute to high pozzolanic reactivity and microstructural refinement, which results in early strength gain and matrix densification [3]. Shihada & Arafa [4] observed a 60% increase in 28-day compressive strength of UHPC with an optimum 15% silica fume content of cement mass compared to the specimens with zero content of silica fume, while Wu et al. [5] observed a significant increase of 10–25 MPa in the 28 days compressive and flexural strengths of UHPC containing 15%–25% silica fume when compared to that of the reference sample. This strength enhancement was attributed to a refined microstructure, which reduces the overall porosity of the concrete matrix. Zheng et al. [6] reported that the addition of 10% silica fume in ultra-high performance fibre reinforced concrete (UHPFRC) densified the matrix and interfacial transition zone (ITZ), leading to higher peak load and fracture energy in four-point bending tests. Whereas matrix densification became the main contributing factor at higher contents (≥20%). Szcześniak et al. [7] experimentally evaluated the performance of UHPC mixtures with the addition of MS in the amount of 6.7%–14.7% and fly ash (FA) in the amount of 8.3%–26.7%. The best strength properties were obtained for concrete containing 16.7% FA and 13.3% MS, achieving above 120 MPa and 150 MPa compressive strength after 28 and 90 days of standard curing, respectively. Collectively, these studies confirm the effectiveness of micro silica or silica fume in achieving UHPC's mechanical performance; however, its high cost, limited availability, and environmental burden motivate the investigation of alternative and supplementary binder systems.

In comparison, fly ash performance in UHPC remains limited. This is mainly due to its slow pozzolanic reaction, which results in low early-age strength, along with variability in its composition. Nevertheless, Jing et al. [8] found that FA enhances rheology and also provides long-term strength benefits in UHPC mixtures. Bahedh et al. [9] observed an increase in the workability of the UHPC as the dosage of FA increased from 0% to 40%. Mix with 40% FA as a replacement of cement showed a notable strength gain of 122.4 MPa after 28 days of curing. Fu et al. [10] assessed the performance of 0%–100% FA as a cement substitute on the drying shrinkage of UHPC. The results showed that adding FA reduces the drying shrinkage of UHPC without compromising the compressive strength, and this effect can be strengthened by increasing the dosage within the tested range. The sample containing

100% FA exhibits the lowest drying shrinkage; compared to the sample without FA, the shrinkage was reduced by 38.46% after 7 days and 14.57% after 28 days of curing. Recent research further supports its value: Van Tuan et al. [11] developed a mix design for UHPC using high-volume fly ash (HVFA) (>50%) in mix design. The experimental results showed achieving compressive strengths of >120 MPa (standard curing) and >150 MPa (heat treatment), while reducing embodied CO_2 emissions by 56.4%. These findings highlight the potential of FA to enhance sustainability and long-term performance; however, achieving adequate early-age strength while maintaining reduced cement content remains a key challenge in UHPC mix optimization.

From a sustainability point of view, reducing the high cement content in UHPC through SCM replacement is a growing research priority. Waste glass powder (WGP), owing to its high amorphous silica content and latent pozzolanicity, has attracted attention as a potential alternative. Soliman and Tagnit-Hamou [12] investigated the properties of UHPC specimens by replacing cement with 10%, 20%, 30%, 40%, and 50% of glass powder (GP) by weight and 50% and 100% quartz powder with GP. The UHPC specimens prepared with cement and silica fume were considered as the control specimens. It was noted that the compressive strength of concrete specimens with GP exhibited slightly higher strength compared to the control specimens. Mohamed et al. [13] investigated the use of 10%, 20%, 30%, and 40% of WGP, derived from grinding glass waste, as an SCM to replace OPC and silica fume in UHPC. The specimens were tested following a three-point loading test. It was noted that the flexural strength for the case of specimens having 0%, 10%, 20%, 30%, and 40% WGP was found to be 18.2, 20.1, 27.9, 17.4, and 14.4 MPa. Thus, indicating that the 20% glass-cement replacement specimen showed the highest flexural resistance. While Taha and Nounu [14] used recycled glass sand (RGS) in 0%, 50%, and 100% replacement proportions, primarily as an inert filler, and observed no significant differences in the compressive strength of the concrete. Sharifi et al. [15] investigated the use of ground waste glass (GWG) microparticles as a partial replacement for cement in self-consolidating concrete (SCC), examining various mechanical and durability properties. The study concluded that incorporating up to 15% GWG microparticles enhances the workability and mechanical properties of SCC. Several studies have used WGP in concrete; research on its high-volume application as a reactive SCM, particularly in combination with MS or FA, remains limited. Recent studies, such as Jalalinejad et al. [16] achieved the highest increase in the compressive, tensile, and flexural strengths (16.99%, 23.53%, and 17.65%, respectively) of SCC, containing 22.5% glass powder and 10% silica fume. In comparison, concrete with 30% glass powder showed a slight reduction in the strength parameters. However, it still performed better than the control mix, emphasizing WGP's potential for sustainable UHPC mix designs. Despite these efforts, the high-volume application of WGP as a reactive SCM in UHPC, particularly in combination with MS or FA has remained insufficiently explored.

Fibres in UHPC play a critical role in enabling post-cracking toughness and strain capacity in UHPC. Prem et al. [17] performed an experimental study to evaluate the mechanical properties of UHPC by preparing specimens with the steel fibre percentage of 2%–2.5% and aspect ratios of 40 and 81 after 28 days of curing. It was observed that the compressive strength for different mixes was in the range of 93–180 MPa. Wu et al. [18] evaluated the performance of three different types of steel fibre (straight, hooked-end, and corrugated) and fibre volumes of 0, 1%, 2%, and 3% on the concrete compressive strength. It was noted that the compressive strength of the specimens without fibre was found to be 105 MPa, which increased to 150 MPa when specimens with a higher fibre volume of 3% straight steel fibres were used. Furthermore, it was also observed that the specimens with 3% corrugated fibres and hooked end exhibited 59% and 48% higher compressive strength, respectively, compared to the specimens with an equal amount of straight fibres. Sharobim et al. [19] studied

the effect of steel fibre content in the range of 0%–3% by volume on the mechanical properties of UHPC specimens. It was found that after 28 days of curing, the maximum compressive strength of 123.5 MPa, which was 23.5% higher than the specimen cast as a control. Prem et al. [20] conducted an experimental study using different steel fibre volumes and aspect ratios (2.5% and 2.0% of 13 mm and 6 mm length fibres with a diameter of 0.16 mm) to examine the stress-strain behaviour, tensile behaviour, and flexural behaviour under various curing regimes. It was observed that a maximum 28-day compressive strength of 144 MPa was achieved in the specimen with 2% steel fibres under water curing. It was concluded that adding steel fibres to UHPC increased both toughness and strain at peak stress and that this behaviour is directly proportional to the reinforcement index (RI). Le Hoang and Fehling [21] examined the effect of steel fibre contents (1.5% and 3%) with different aspect ratios on the uniaxial tensile and compressive behaviour of UHPC. It was observed that the incorporation of steel fibre reduces the flowability with insignificant change in the compressive strength and the elastic modulus. However, the post-peak branch in the stress–strain curve is substantially influenced by the increase in the fibre content, and fibres with a higher aspect ratio may lead to a better improvement of post-peak behaviour. The linearity of the stress–strain curve was found to be 79% and 80%–85% of the compressive strength for UHPC and UHPFRC, respectively. These observations indicate that fibre efficiency depends on both fibre volume fraction and aspect ratio, commonly calculated using the reinforcement Index (RI), which provides a rational basis for comparing different fibre-reinforced UHPC systems.

While steel fibres have been extensively investigated for strength enhancement in UHPC, synthetic fibres such as polypropylene (PP) are primarily incorporated to control microcrack initiation and propagation rather than to improve mainly compressive strength. Owing to their low elastic modulus, PP fibres contribute marginally to load-carrying capacity; however, they are highly effective in mitigating drying shrinkage and improving strain capacity through crack bridging and crack control mechanisms. By restraining microcrack growth at early stages, PP fibres delay crack localization, reduce crack widths, and enhance deformation capacity [22].

The performance of PP fibres is strongly influenced by fibre geometry. Crimped (wave-shaped) PP fibres provide improved mechanical anchorage within the cementitious matrix compared to straight fibres, resulting in higher pull-out resistance and more stable fibre–matrix interaction. This enhanced bonding enables sustained stress transfer across cracks and more effective crack control, despite the low stiffness of PP fibres [23].

Several studies have reported secondary improvements in compressive strength at limited PP fibre contents. He et al. [24] experimentally evaluated the effect of different types of fibres, which include high-performance polypropylene (HPP) fibre and glass fibre (GF), on the compressive strength of concrete. After 28 days of curing, the maximum compressive strength of 108.24 MPa was achieved by the HPP-UHPC specimen. It was observed that 2% fibre content in UHPC provides better mechanical properties. Sohaib et al. [25] investigated the influence of 0%–4.5% PP on the compressive strength of concrete. It was noted that after 7 and 28 days of curing, the addition of PP fibres increased the compressive strength by 20% and 16%, respectively, when compared with control specimens. It was also noted that the compressive strength increased when fibres of up to 1.5% were used in preparing concrete specimens. However, beyond 1.5% the compressive strength decreases. Ramujee [26] studied the compressive and tensile strength of PP fibre-reinforced concrete specimens using fibre in the range of 0% to 2%. It was observed that the maximum increase of 34% in the compressive strength and 40% in the splitting tensile strength was achieved with the increase in volume ratios of PP fibres as compared to the control specimen. Aly et al. [27] investigated PP fibre concretes (0%–0.5% volume) and reported effective control of early-age shrinkage cracking.

In high-strength concretes, Bouziadi et al. [28] experimentally investigated the total shrinkage and mechanical properties of the high strength concrete (HSC) containing steel fibres, considering two aspect ratios (55, 80), PP fibres, and hybrid fibres (HF). The results showed that PP fibres consistently reduce visible shrinkage cracks even at low dosages (0.2%–0.5%) than the steel fibres. By the addition of 0.2% of PP fibres, the reduction is 31% under the curing temperature of 20°C. Although several studies have examined the performance of straight or crimped PP fibres in normal and high-performance concretes, their application in UHPC, particularly crimped PP fibres, has not been systematically investigated. This leads to a limited understanding of their mechanical characteristics, fibre concrete matrix interaction, and post-cracking behaviour in UHPC. Therefore, this gap highlights the need to study the effect of crimped PP fibres in UHPC, with particular emphasis on their mechanical performance, ductility, and crack bridging efficiency.

Globally, damage-based constitutive models have been extensively developed for conventional and high-performance concretes. However, their direct application to the complex mechanical behavior of fibre-reinforced UHPC, influenced by multi-type fibres and SCMs, have not be fully captured by traditional stress–strain models. Most existing models fail to capture UHPC's distinctive post-peak ductility, fibre-bridging effects, and strain-hardening behaviour, or require extensive experimental calibration, thereby limiting their predictive reliability and large-scale applicability. Guo [29] proposed a principal stress–strain model for reinforced concrete, and Saenz [30] provided a continuous compressive response, but both neglected stiffness degradation and microcrack evolution. Xiao et al. [31], Jiao et al. [32], and Ju et al. [33] developed empirical or regression-based fibre-reinforced concrete models, Al-Hassani et al. [34] developed constitutive model for reactive powder concrete, yet these approaches are largely one-dimensional, focus solely on axial compression, and fail to capture post-peak ductility, lateral strain, and fibre–matrix interactions. These limitations highlight the need for constitutive models that can accurately capture multi-phase stress–strain behaviour, fibre-induced effects, post-peak softening, and lateral deformation. In contrast, elasto-damage constitutive modeling offers a robust framework to represent progressive stiffness degradation, microcracking, and fibre bridging, reproducing both pre and post peak branches of the stress–strain curve. By introducing a strain-dependent damage variable, such models account for variations in Poisson's ratio, post-peak softening, and the enhanced ductility provided by different fibres.

Hence, the development and validation of UHPC-specific constitutive models is essential to bridge experimental research with practical design and simulation. Therefore, to address these limitations of existing models, the present study modifies an elasto-damage constitutive model developed by Khan and Zahra [35] and extends its applicability to UHPC containing 20% ultra-fine waste glass powder, microsilica, fly ash, 2% steel fibres, and 1.5% PP fibres, enabling mechanistic predictions of stiffness, ductility, and toughness. The proposed model predicts the monotonic compressive stress–strain behaviour of UHPC using a strain-controlled incremental formulation, thereby enhancing simulation accuracy while reducing experimental dependence. This approach overcomes the key limitations of previous regression-based formulations and provides a reliable predictive tool for numerical analysis, optimized structural design, and the development of sustainable UHPC mixtures. To address these identified gaps, this study evaluates a new UHPC system using unconventional supplementary cementitious materials (SCMs) and synthetic fibres. Research gap identified and novel contributions of this study include:

- Systematic application of crimped PP fibres in UHPC to improve mechanical anchorage, pull-out resistance, and crack bridging.

- High-volume (20%) use of ultra-fine waste glass powder (UFWGP) as SCM systematically combined with MS or FA to optimize binder performance.
- Extension of the reinforcement Index framework to synthetic fibres, enabling rational comparison with steel fibres in UHPC.
- Independent testing of each fibre type in different binder mixes to avoid hybrid effects.
- A comprehensive experimental program of 24 UHPC mixes yielding robust data relating fibres and binder formulations with rheology, mechanical properties, and long-term shrinkage.
- Development and validation of an enhanced elasto-damage constitutive model, adapted from Khan and Zahra [35], specifically modified to capture UHPC's monotonic compressive stress-strain behaviour, concrete damage parameter, post-peak ductility, and fibre bridging effects.

2 Experimental Program

2.1 Mix Designs

This study aims to evaluate the mechanical properties including compressive, splitting tensile and flexural strength of UHPC specimens. For this purpose, two mix designs, i.e., one based on the ACI Committee 239-R18 guidelines [36] (Mix Design A), and the other as proposed by Wu et al. [18] (Mix Design B), were used as control mix designs for producing UHPC. The original ACI Mix Design (Mix Design A) used mass proportions of OPC and silica fume as binders, quartz powder/silica flour, and sand as fine aggregates, with steel fibre as reinforcement. The water-cementitious ratio (w/cm) of 0.20 and a sand-binder ratio (s/b) of 0.9 were proposed to achieve the compressive strength of 150 MPa [36]. A second reference mix design, (Mix Design B), proposed a UHPC mixture containing OPC, silica fume, and sand with a w/cm ratio of 0.2 and a s/b ratio of 1. The Mix Design also evaluated the performance of different shapes of steel fibres and its content.

In the current study, these both original Mix Designs A and B were modified to further improve the properties of the UHPC, by incorporating the micro silica (MS), class F fly ash (FA), and ultra-fine waste glass powder (UFWGP) as SCMs. The physicochemical properties of all the binder materials are provided in Table 1. UFWGP was used at a high replacement level (20%) as a chemically reactive SCM, combined with either micro silica (MS) or fly ash (FA). Fig. 1 shows the particle size distribution curve of UFWGP. Although the original Mix Design B included different steel fibre shapes, the present study only investigated the influence of 2% straight steel and 1.5% crimped polypropylene fibres. Crimped PP fibres were introduced in UHPC, with the hypothesis that their unique geometry enhances fibre anchorage, pull-out resistance, and crack-bridging efficiency. Properties of straight steel fibres having a length of 13 mm and a diameter 0.2 mm and crimped polypropylene fibres were 54 mm long and 0.9 mm in diameter were used in this study to cast UHPC. The properties of both type of fibres are provided in Table 2. The Reinforcement Index (RI) was used to quantify the contribution of fibres to concrete performance by incorporating both type of fibre' content and geometry. It is defined as the product of fibre volume content and aspect ratio (l/d), and is calculated using Eq. (1):

$$RI = V_f \times \frac{l}{d} \tag{1}$$

where V_f is the fibre volume fraction, l is the fibre length, and d is the fibre diameter. For straight steel fibres, the nominal length and diameter are used directly. For crimped or non-circular polypropylene (PP) fibres, an equivalent diameter (d_{eq}) is calculated by Eq. (2) based on the fibre cross-sectional area:

$$d_{eq} = \sqrt{\frac{4A}{\pi}} \tag{2}$$

where A is the cross-sectional area of the fibre. The fibre length corresponds to the straightened length of the crimped fibre to reflect its effective bridging and pull-out potential. The RI values for all tested fibres were calculated using the properties listed in Table 2. The RI value of 2% straight steel fibres is 1.30, while that of 1.5% crimped polypropylene fibres is 0.97, enabling one of the unique quantitative cross-comparisons of synthetic and steel fibre efficiency in UHPC. The high-performance superplasticizer REMICRETE PCSP [37] was also used in preparing the mix designs.

Table 1: Physicochemical properties of binders

Property	OPC	Micro Silica	Class F Fly Ash	UFWGP
Specific gravity	3.15	2.2	2.25	2.45
Specific surface area (m^2/kg)	350	20,000	400	1000
d10 (μm)	3	0.08	4.5	1
d50 (μm)	13	0.2	18	5
d90 (μm)	40	0.9	55	20
Blaine fineness (m^2/kg)	330	—	350	600
BET surface area (m^2/g)	—	20	1.5	3
Loss on ignition (LOI, %)	2	1.5	3.5	0.8
SiO_2 (%)	22.1	94.4	55.3	73.2
CaO (%)	65.6	6.1	3.2	11.3
Al_2O_3 (%)	3.5	1.1	26.2	1.5
Fe_2O_3 (%)	4.3	0.6	7.2	0.4
$Na_2O + K_2O$ (%)	0.87	1.2	2.1	13.5
MgO (%)	1.92	0.42	1.5	3.98
SO_3 (%)	2.35	0.21	0.5	0.26
TiO_2 (%)	0.21	0.3	0.5	0.05
Amorphous content	Moderate	Very high	High	Predominantly amorphous

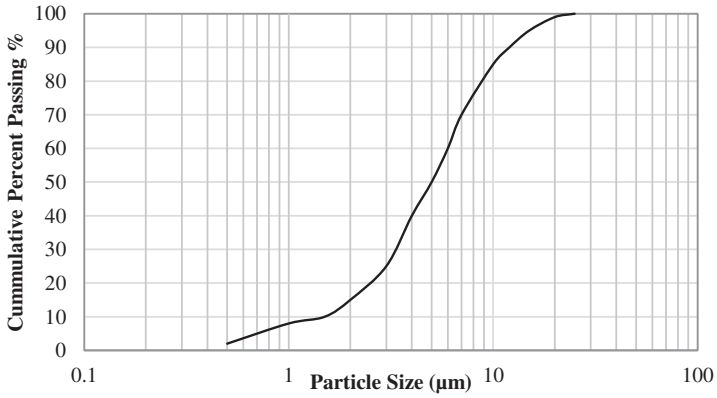

Figure 1: Particle size distribution curve of UFWGP

Table 2: Physical properties steel and polypropylene fibres used

Fibres	Steel fibre [38]	Polypropylene fibre [39]
Unit weight	7850 kg/m^3	910 kg/m^3
Material	Brass coated carbon steel	Polypropylene polymer
Length	13 mm	54 mm
Diameter	0.2 mm	0.9 mm
Thickness	–	0.6 mm
Width	–	1.1 mm
l/d ratio	65	60
Area	0.0314 mm^2	0.66 mm^2
Tensile strength	2300 MPa	≥460 MPa
Modulus of elasticity	250 GPa	4 GPa
Alkali resistance	High	Strong
Max temperature	1000°C	≥160°C

Initially, specimens were cast with 100% micro silica without fibres. The same specimens were then cast using 20% replacement of cement (by weight) with UFWGP. These mixes were considered control specimens. After casting the control specimens, the next step involved adding 2% micro straight steel fibres and 1.5% polypropylene fibres to the concrete mixes, as shown in Table 3. Finally, the same trials were repeated, replacing micro silica with 100% fly ash. A high-strength polycarboxylic ether-based water reducing superplasticizer was used to attain a mini-slump flow of ≥160 mm [40].

Table 3: Mix proportion of UHPC (kg/m^3)

Mix design	Mix ID	OPC	MS	FA	UFWGP	S	W	SP	W/B	Fibre	
										SF	PP
A	**A1**	800	311.2	0	0	1111	222.2	22	0.2	0	0
	A2	640	311.2	0	160.0	1111	222.2	22	0.2	0	0
	A3	800	311.2	0	0	1111	222.2	22	0.2	157	0
	A4	640	311.2	0	160.0	1111	222.2	22	0.2	157	0
	A5	800	311.2	0	0	1111	222.2	22	0.2	0	13.7
	A6	640	311.2	0	160.0	1111	222.2	22	0.2	0	13.7
	A7	800	0	311.2	0	1111	222.2	22	0.2	0	0
	A8	640	0	311.2	160.0	1111	222.2	22	0.2	0	0
	A9	800	0	311.2	0	1111	222.2	22	0.2	157	0
	A10	640	0	311.2	160.0	1111	222.2	22	0.2	157	0
	A11	800	0	311.2	0	1111	222.2	22	0.2	0	13.7
	A12	640	0	311.2	160.0	1111	222.2	22	0.2	0	13.7
B	**B1**	792	264	0	0	1056	211.2	21.1	0.2	0	0
	B2	634	264	0	158.4	1056	211.2	21.1	0.2	0	0
	B3	792	264	0	0	1056	211.2	21.1	0.2	157	0

(Continued)

Table 3 (continued)

Mix design	Mix ID	OPC	MS	FA	UFWGP	S	W	SP	W/B	Fibre	
										SF	PP
	B4	634	264	0	158.4	1056	211.2	21.1	0.2	157	0
	B5	792	264	0	0	1056	211.2	21.1	0.2	0	13.7
	B6	634	264	0	158.4	1056	211.2	21.1	0.2	0	13.7
	B7	792	0	264	0	1056	211.2	21.1	0.2	0	0
	B8	634	0	264	158.4	1056	211.3	21.1	0.2	0	0
	B9	792	0	264	0	1056	211.2	21.1	0.2	157	0
	B10	634	0	264	158.4	1056	211.3	21.1	0.2	157	0
	B11	792	0	264	0.0	1056	211.2	21.1	0.2	0	13.7
	B12	634	0	264	158.4	1056	211.3	21.1	0.2	0	13.7

Note: OPC: Ordinary Portland Cement, MS: Micro Silica/ Silica Fume FA: Fly Ash, UFWGP: Ultra-fine waste glass powder, S: Sand, W: Water, SP: Superplasticizer, w/b: Water-to-binder ratio, s/b: sand-binder ratio, SF: Steel fibres, PP: Polypropylene fibres.

2.2 Mixing Procedure

To ensure optimal mixing and consistency of UHPC specimens, the raw materials were mixed as per the procedure outlined in the [41]. For the preparation of UHPC mix, a high-speed concrete mixer was used. Sand was first added and mixed for about 90 s at a speed of 2 revolutions per second (rps) to improve uniform particle dispersion and prevent agglomeration of fine sand particles, ensuring a homogeneous mixture. The dry materials, including cement and SCMs, were then added and further mixed for 90 s at the same speed to assure proper blending. This was followed by adding 90% of the required superplasticizer in the 90% of the required water, and this solution was added and thoroughly dispersed in the dry materials. The mixture was then mixed for 120 s at a speed of 4 rps.

Following that, the remaining superplasticizer and water were added and then mixed for another 240 s at the same speed until the UHPC transitioned from a dry powder to a fluid mixture. In the final step, fibres were added gradually to make sure uniform distribution throughout the mixture to avoid agglomeration. The UHPC mixture was then additionally mixed for 120 s at the speed of 6 rps. The mixing process was carefully controlled so that the temperature of the UHPC did not rise considerably. Chilled water was utilized in the mixing, and the mixing speed was maintained throughout to avoid increasing the temperature, which could result in more stiffness than desired.

2.3 Casting and Curing

Specimens were cast into moulds as follows: cylinders (100 mm × 200 mm) for compressive and splitting tensile tests, beams (100 mm × 100 mm × 500 mm) for flexural tests, and prisms (25 mm × 25 mm × 275 mm) for drying shrinkage. Each mix had three specimens per test. Specimens were compacted using vibration to remove entrapped air. All the specimens were then cured under standard normal curing conditions for 28 days at 20 ± 2°C and >95% relative humidity. Drying shrinkage specimens were cast, cured and monitored for 98 days under controlled conditions.

2.4 Fresh State Tests

In this study, flow table and viscosity tests were carried out for all Mix Designs reported in Table 3. The flow table test was conducted using ASTM C1437-20 [42] standard, whereas, the TBT-Z6 type

F1 rotational viscometer was used to observe and measure the viscosity of the UHPC mixes using standard ASTM D2196-18 [43].

2.5 Hardened State Tests

To evaluate the hardened state properties of the concrete specimens, compressive strength, modulus of elasticity, splitting tensile strength and flexural strength tests were conducted after 28 days curing, using ASTM Standards C39/C39M-20 (2020) [44], ASTM C469/C469M-14 (2014) [45], C496/C496M-17 (2017) [46], C78/C78M-10 (2018) [47], respectively. The drying shrinkage test was also performed following ASTM C157/C157M-17a [48] standard to investigate the behaviour of UHPC during its drying and curing period.

3 Results and Discussion

Results of all the tests conducted to determine the fresh and hardened state properties are discussed in the following sections.

3.1 Fresh State Properties

3.1.1 Flowability

Fig. 2 and Table 4 show the measured flows exhibited by UHPC mixes considered herein. It can be noticed from Table 4 that mixes having micro silica and UFWGP (which has low water absorption ability and smoother surfaces) exhibited increased flowability as compared to the corresponding mixes without UFWGP. This behaviour is attributed to the fact that the flat surface of the UFWGP improves the flowability, hence, allowing the concrete to flow easily [15]. Furthermore, the increased workability is also associated with the addition of UFWGP which results in cement dilution that helps to reduce the cement hydration products in the initial period of mixing [49].

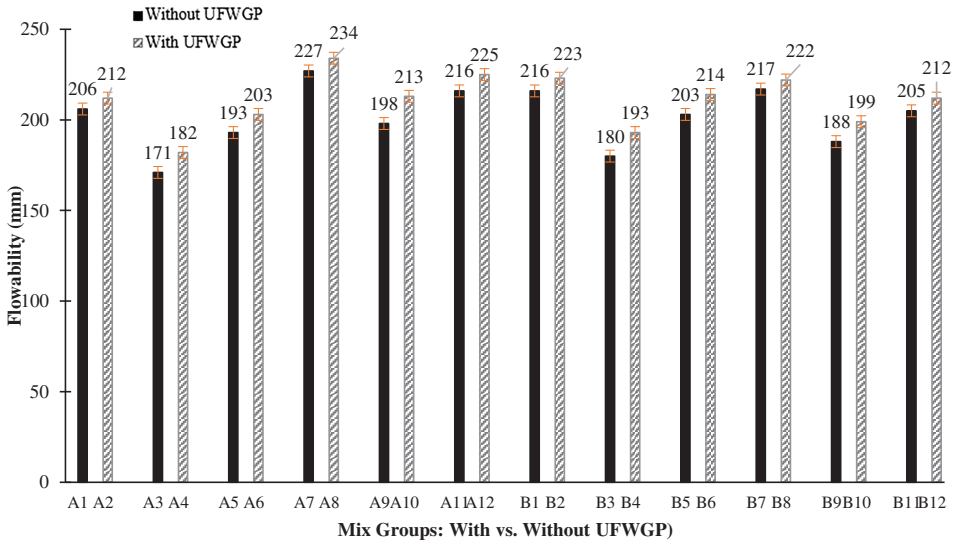

Figure 2: Flowability of different mixes of UHPC specimens

Table 4: Fresh state properties of UHPC

Mix ID	Flow (mm)	Viscosity (Pa.s)
A1	206	31
A2	212	28
A3	171	48
A4	182	44
A5	193	36
A6	203	31
A7	227	22
A8	234	19
A9	198	34
A10	213	27
A11	216	26
A12	225	23
B1	216	26
B2	223	24
B3	180	45
B4	193	37
B5	203	31
B6	214	27
B7	217	26
B8	222	24
B9	188	40
B10	199	33
B11	205	30
B12	212	28

It should be noted that micro silica content remained constant across these mixes. Micro silica alone (without UFWGP) generally increases the water need due to its extremely fine particle size and high specific surface area, which decreases the concrete mix flowability. Furthermore, it was also observed that with the addition of steel fibres in the mixes, the flow value decreases compared to the control mixes without steel fibres, as well as with PP fibres. This is due to the high RI and fibre density of steel fibres, which reduces flowability due to higher rigidity compared to the PP fibres. This trend is in line with the trend reported by Wu et al. [18].

It can also be observed from Fig. 2 and Table 4 that the use of fly ash in place of micro silica resulted in increased flowability for all the mixes. This is attributed to the fact that the fly ash particles are spherical in shape and have a lower density than the cement particles, thus enhancing the flowability of the concrete mix by filling voids and decreasing friction between the particles.

3.1.2 Viscosity

The plastic viscosity exhibited by UHPC mixes investigated herein is shown in Fig. 3 and Table 4. In general, for the UHPC mixes tested, the plastic viscosity decreases with the increase in flowability.

It is vital to observe that with the inclusion of micro silica in the UHPC mixes, the flow of fresh UHPC decreases due to its high fineness and surface area, resulting in an increase in plastic viscosity. As a result, the highest plastic viscosity was attained in mixes A1 to A6 and B1 to B6, which contained micro silica. This conforms to the findings of Galobardes et al. [50], who reported that the addition of micro silica significantly increases the water demand in cementitious mixes.

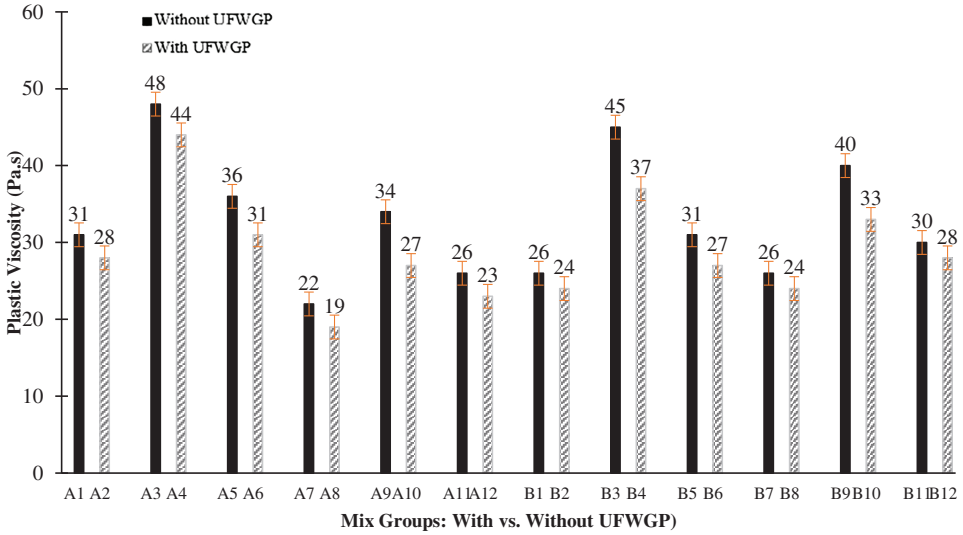

Figure 3: Plastic viscosity of different mixes of UHPC specimens

In contrast, the spherical "ball-bearing" effect of fly ash improves flowability and reduces viscosity, as observed in mixes A7 to A12 and B7 to B12 and shown in Fig. 3. To increase the flowability of UHPC, fly ash can perform as an inorganic agent that reduces viscosity; however, the consistency coefficient of UHPC paste steadily decreases with the addition of fly ash.

Furthermore, when OPC is partially replaced with the UFWGP, the paste exhibits a decrease in plastic viscosity. This occurs because UFWGP possesses a lower specific gravity than cement. As a result, the solid-to-water ratio (by volume) becomes greater in the UHPC blend containing both cement and UFWGP, resulting in improved rheological characteristics compared to the blend with only cement.

In addition, it was also noted that the UHPC mixes prepared with a steel fibres having high RI exhibited a reduction in flowability, and a similar effect was observed in the case of crimped polypropylene fibres, indicating that both types of fibre significantly influence the fresh rheology of UHPC.

3.2 Hardened State Properties

Results of all the hardened state properties of UHPC i.e., compressive strength, modulus of elasticity, splitting tensile and flexural strength are presented in this section.

3.2.1 Compressive Strength

The average compressive strength test results of all the UHPC mixes are given in Table 5. It can be noticed from Table 5 that mixes with UFWGP exhibited higher strengths as compared to the mixes without UFWGP, irrespective of fibre type and other SCM, i.e., micro silica and fly ash. Mixes with

micro silica exhibited higher strength as compared to mixes with fly ash, irrespective of fibre type. Furthermore, mixes with steel fibres exhibited higher strengths as compared to mixes with PP fibres.

Table 5: Compression strength test results of UHPC at curing age of 28 days

Mix ID	f'_c (MPa)			Strain (mm/mm)		Ductility (μ)	Total Toughness (MPa·strain)	E_o(GPa) (mean ± SD)
	Exp (mean ± SD)	Pre	*Relative residual* %	Peak	Ultimate			
A1	96.5 ± 2.4	95.8	0.69	0.002350	0.002530	1.08	0.141	42.50 ± 2.76
A2	102.3 ± 4.1	102.0	0.25	0.002408	0.002690	1.12	0.155	43.61 ± 1.47
A3	134.1 ± 3.7	140.0	−4.19	0.003094	0.012360	4.00	0.782	47.30 ± 2.16
A4	144.8 ± 4.1	141.3	2.45	0.003393	0.013856	4.08	1.021	49.77 ± 2.55
A5	125.5 ± 4.7	132.4	−5.20	0.002728	0.006200	2.27	0.344	44.86 ± 3.29
A6	129.7 ± 3.3	136.5	−4.99	0.002770	0.007100	2.56	0.425	46.06 ± 1.43
A7	76.4 ± 3.9	78.6	−2.80	0.002111	0.002392	1.13	0.122	38.74 ± 2.25
A8	83.2 ± 4.1	84.1	−1.09	0.002244	0.002468	1.10	0.148	40.01 ± 3.53
A9	122.2 ± 4.6	129.6	−5.73	0.002636	0.010000	3.79	0.688	44.12 ± 2.80
A10	126.1 ± 2.8	135.8	−7.16	0.002697	0.011000	4.08	0.939	44.89 ± 2.03
A11	112.4 ± 4.2	113.1	−0.60	0.002502	0.005600	2.24	0.283	41.32 ± 3.46
A12	117.3 ± 3.3	121.3	−3.34	0.002605	0.006460	2.48	0.363	42.57 ± 3.53
B1	92.0 ± 3.6	91.0	1.09	0.002347	0.002482	1.06	0.135	41.33 ± 3.87
B2	99.9 ± 4.9	97.9	2.04	0.002373	0.002625	1.11	0.146	42.08 ± 2.41
B3	125.1 ± 4.5	130.3	−4.00	0.002725	0.010090	3.70	0.693	45.60 ± 1.12
B4	129.7 ± 3.6	136.5	−4.99	0.002806	0.011009	3.92	0.892	46.31 ± 2.09
B5	117.0 ± 3.3	119.3	−1.91	0.002586	0.005466	2.11	0.276	44.03 ± 3.45
B6	122.6 ± 2.9	126.9	−3.36	0.002657	0.006203	2.33	0.379	45.18 ± 2.98
B7	72.4 ± 4.6	74.5	−2.77	0.002020	0.002227	1.10	0.115	37.12 ± 2.18
B8	77.2 ± 3.4	77.2	−0.03	0.002221	0.002426	1.09	0.137	37.49 ± 3.23
B9	112.1 ± 2.1	112.4	−0.25	0.002473	0.008607	3.48	0.598	40.82 ± 2.11

(Continued)

Table 5 (continued)

Mix ID	f'_c (MPa)			Strain (mm/mm)		Ductility (μ)	Total Toughness (MPa·strain)	E_o(GPa) (mean ± SD)
	Exp (mean ± SD)	Pre	*Relative residual* %	Peak	Ultimate			
B10	120.3 ± 3.9	126.2	−4.66	0.002612	0.010144	3.88	0.845	43.68 ± 1.99
B11	105.0 ± 3.3	102.0	2.90	0.002430	0.004813	1.98	0.276	40.89 ± 2.30
B12	114.1 ± 2.7	115.8	−1.50	0.002562	0.005719	2.23	0.354	42.33 ± 2.27

For mixes A1 to A6, the maximum strength was achieved by A4, having micro silica, UFWGP and steel fibres. The gain in strength was 50% more than A1 and 41.5% more than A2, the mixes without fibres. Similar trend was observed for mixes A7 to A12, where maximum strength was attained by A10, having fly ash, UFWGP and steel fibres, with 65% more strength than A7 and 52% more than A8. In Mix Design A, the specimens reinforced with fibres achieved compressive strength more than 120 MPa (A3 to A6 and A9 to A10), which is the minimum criterion of UHPC in ACI [36], except the specimens with PP fibres (A11 & A12).

For mixes B1 to B6, maximum strength was achieved by B4, having fly ash, UFWGP and steel fibres (41% more than B1 and 30% more than B2). Similar trend was observed for mixes B7 to B12, where maximum strength was attained by B10, having fly ash, UFWGP and steel fibres. The increase in strength was 66% more than B7 and 58% more than B8 mixes. In Mix Design B, the specimens reinforced with fibres achieved compressive strength greater than or close to 120 MPa (B3 to B6), which is the minimum criteria of UHPC in ACI [36], whereas, in mixes, B9 to B12, only B10 attained the minimum desired strength of 120 MPa.

While comparing the results of Mix Design B specimens prepared with micro silica and fly ash, a trend similar to Mix Design A was observed. This is attributed to the fact that the micro silica having high pozzolanic activity led to the higher level of C-S-H gel and resulting in the denser microstructure, thus increasing the concrete compressive strength [6]. Fig. 4 shows the compression test specimens reinforced with steel and PP fibres, and the stress-strain relationships of all the mixes are presented in Fig. 5.

Overall, the stress-strain response of mixes with similar materials used was found to be similar as can be seen in Fig. 5. Mixes with no fibres showed a brittle failure after reaching peak stress with no strain softening in post-peak region. Mixes with PP fibres exhibited low peak stresses as compared to mixes with steel fibres. Both showed strain softening, with mixes containing steel fibres showed higher ductility. Mixes with micro silica demonstrated high peak stresses as compared to the mixes with fly ash. Mixes without fibres showed low initial stiffness as compared to mixes with fibres, irrespective of the fibre type. Mixes with fibres showed almost similar pre-peak response, irrespective of the fibre type used.

(a) (b)

Figure 4: Compressive strength test specimens of UHPC (a) steel (b) PP fibres

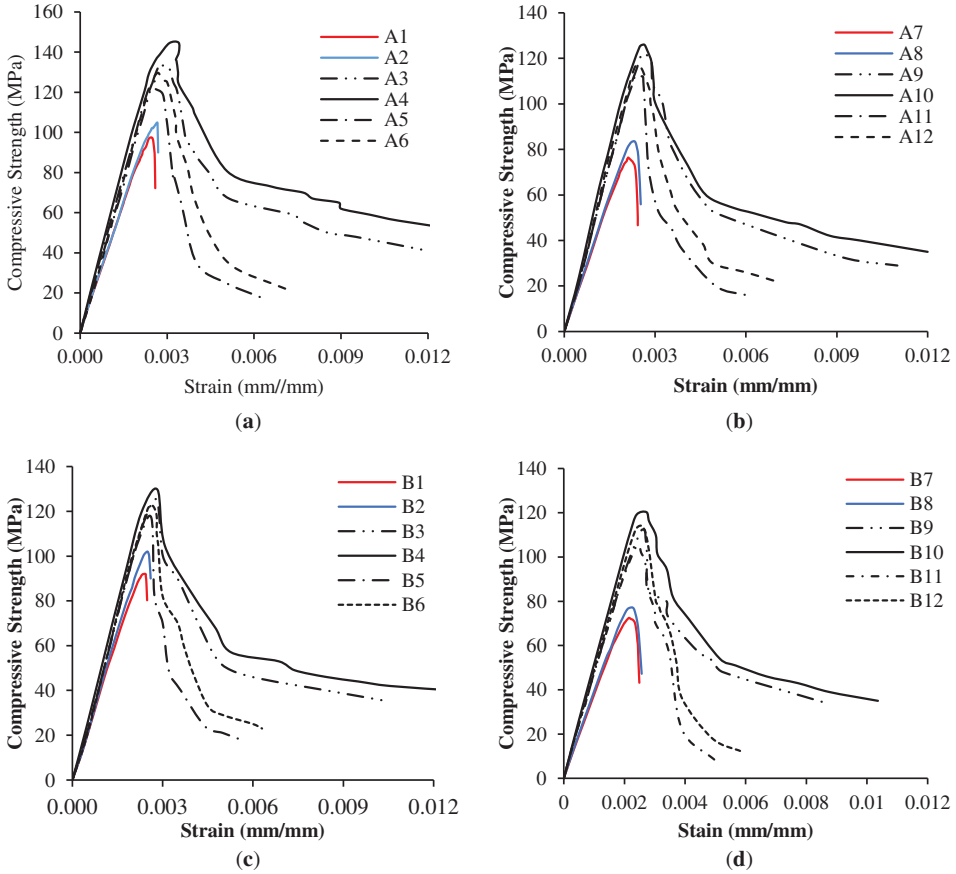

Figure 5: Compressive strength results of UHPC mixes: (a) Mix A-microsilica, (b) Mix A-Class F fly ash, (c) Mix B-microsilica, and (d) Mix B-Class F fly ash

It can be noticed from Fig. 5a, that the mixes with steel fibres exhibited higher strains at failure resulting in higher ductility as compared to the control mixes without fibres. This can be attributed to the fact that straight micro steel fibres prevent rapid propagation of cracks and effectively bridge cracks within the concrete mix, which allows UHPC specimens to deform more before failure. Mix designs with PP fibres also demonstrated similar pattern with peak strains and ductility lower as compared to mixes with steel fibres but higher than control mixes. Fig. 5a–d shows that steel fibres increased ductility and peak strain, while PP fibres provided moderate improvements compared to control mixes. Both Mix Designs A and B followed similar trends.

When comparing the performance of mix designs, A and B, it was observed that the Mix Design A performed better. This may be attributed to the higher density of Mix Design A, as density directly affects the concrete compressive strength due to its denser, void less structure. It is important to note that out of all the specimens investigated, a maximum 28 days compressive strength of 144.8 MPa was obtained by mix A4 which was prepared with micro silica, UFWGP and steel fibres, followed by a compressive strength of 129.7 MPa that was obtained by mixA6, prepared with micro silica, UFWGP and PP fibres.

When comparing the results achieved in the present study with those from the adopted mix designs, it was observed that the specimens cast using the ACI mix design achieved a maximum compressive strength of 144.8 MPa, which was less than the reported strength in the original study. This difference may be due to the factors such as change in fibre shape and dosage. Furthermore, differences may also be attributed to curing methods (normal curing vs. heat curing in the reference study). while the ACI mix design specimens were subjected to heat curing. In comparison, the second mix design in the present study attained a maximum compressive strength of 129.7 MPa, whereas the original study reported 150 MPa. This difference in strength may be attributed to variations in material quality and chemical composition, including difference in cement, SCMs, aggregates and/or fibres.

3.2.2 Modulus of Elasticity (MOE)

The modulus of elasticity (MOE) is defined as the slope of the stress–strain curve (σ–ε) in the elastic deformation region [51]. The modulus of elasticity at 28 days of all the specimens cast using mix designs A and B was determined based on ASTM-C469/C469M-14 [45] and is presented in Table 5. A trend like compressive strength can be noticed from Table 5, where both mix designs with UFWGP exhibited higher MOE as compared to the mixes without UFWGP, irrespective of fibre type and other SCM, i.e., micro silica and fly ash. Mixes with micro silica exhibited higher MOE as compared to mixes with fly ash, irrespective of fibre type. Furthermore, mixes with steel fibres exhibited higher MOE as compared to mixes with PP fibres. Both the mix designs A and B demonstrated a similar trend.

3.2.3 Splitting Tensile Strength (STT)

Splitting tensile strengths (STT) exhibited by the mix designs A and B are presented in Table 6. Fig. 6 shows the splitting tensile test specimens reinforced with steel and PP fibres. Fig. 7, demonstrating the influence of the different types of SCMs and fibres on the splitting tensile strength of UHPC specimens. Generally, the tensile strength of UHPC is around 8 MPa, but the inclusion of fibres increases this value, enhancing the strength up to approximately 15 MPa [52]. From the results of all the UHPC mixes given in Table 6, it is evident that the fibre type and volume fraction have an important effect on the splitting tensile strength of concrete.

Table 6: Splitting tensile and flexural strength test results of UHPC at curing age of 28 days

Mix ID	Splitting tensile strength (f'_t) (MPa) (mean ± SD)	Flexural strength f'_f (MPa) (mean ± SD)
A1	8.0 ± 0.7	11.7 ± 0.7
A2	8.8 ± 0.5	12.9 ± 0.8
A3	11.5 ± 0.6	24.8 ± 1.5
A4	12.7 ± 0.4	30.1 ± 1.8
A5	9.6 ± 0.5	13.0 ± 0.8
A6	10.6 ± 0.4	15.2 ± 0.7
A7	6.0 ± 0.7	7.3 ± 0.6
A8	6.8 ± 0.4	10.6 ± 0.5
A9	7.9 ± 0.6	15.9 ± 1.0
A10	8.5 ± 0.5	18.7 ± 0.9
A11	6.9 ± 0.3	10.9 ± 0.7
A12	7.8 ± 0.5	12.3 ± 0.6
B1	7.6 ± 0.4	11.1 ± 0.8
B2	8.3 ± 0.6	12.1 ± 0.7
B3	10.1 ± 0.5	23.0 ± 1.4
B4	11.2 ± 0.4	28.8 ± 1.7
B5	8.9 ± 0.7	11.7 ± 0.7
B6	9.9 ± 0.6	12.9 ± 0.8
B7	5.0 ± 0.5	6.2 ± 0.4
B8	5.9 ± 0.4	9.3 ± 0.5
B9	6.4 ± 0.6	15.4 ± 1.0
B10	7.8 ± 0.7	17.5 ± 0.8
B11	5.8 ± 0.5	9.7 ± 0.5
B12	7.0 ± 0.4	11.8 ± 0.9

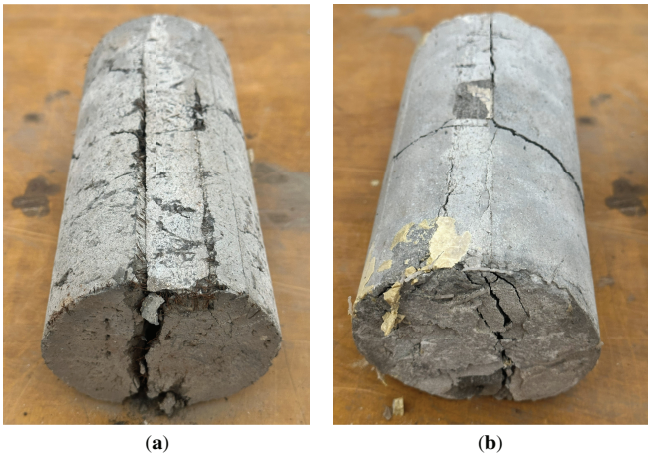

(a) (b)

Figure 6: Splitting tensile strength test specimens of UHPC (a) steel (b) PP fibres

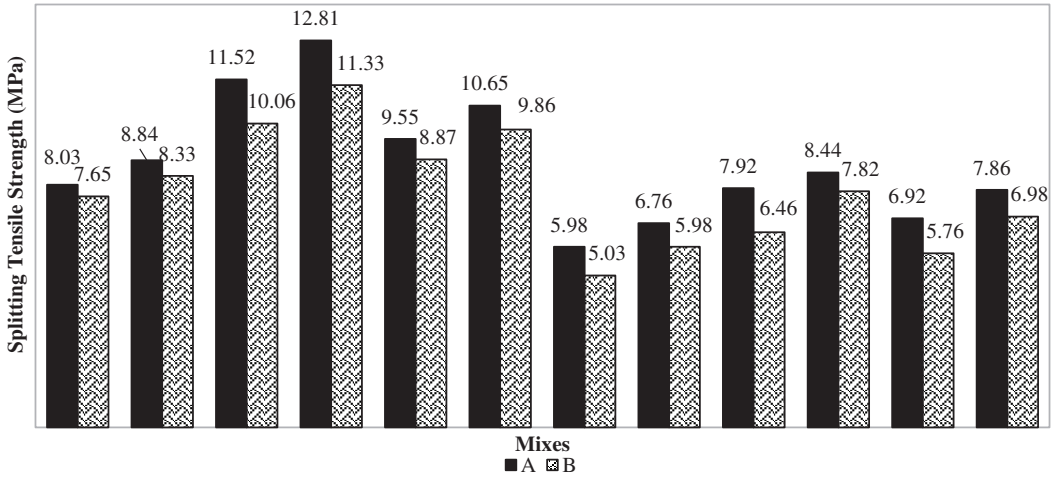

Figure 7: Splitting tensile strength test results of UHPC specimens

A trend like compressive strength and MOE was again observed in the case of STT. Steel fibres, due to their higher tensile strength and stiffness than PP fibres and their ability to effectively bridge cracks under tensile load, resulted in a substantial improvement in the tensile strength as compared to PP fibres. PP fibres, being less stiff and having lower tensile strength, primarily help to control micro-cracks and improve ductility rather than significantly enhancing the tensile strength. Overall, the results are in good agreement with previous studies, highlighting the significant role of fibre type and content in improving the STT of UHPC specimens.

3.2.4 Flexural Strength

Flexural strength test results of specimens prepared using mix designs A and B, was determined using a three-point bending test in accordance with ASTM C78/C78M-10 [47], is presented in Table 6, with corresponding load-displacement curves in Fig. 8. Flexural strength followed a trend like other mechanical properties. Specimens with steel fibres exhibited higher flexural capacity than those with PP fibres, irrespective of the SCM used. This improvement is attributed to the higher tensile strength and crack-bridging ability of steel fibres. The use of steel fibres also improves fibre distribution in the concrete matrix [52], leading to controlled crack propagation. In contrast, PP fibres likely reduced flexural strength due to strong interactions between the longer fibres, which disrupt alignment and reduce their ability to carry the flexural load [53]. Fig. 9 shows the flexural strength test specimens reinforced with steel and PP fibres.

The overall load-displacement response of the specimens with the same materials showed similar behaviour. Specimens without fibres exhibited low initial stiffness, brittle failure after peak load, with the load-carrying capacity dropping to zero, unlike specimens with fibres. Specimens containing fly ash showed lower flexural strength than those with micro silica due to the slower early-age strength development of fly ash. Micro silica specimens demonstrated high peak loads compared to fly ash, with an almost similar post-peak response. The addition of UFWGP further improved the flexural response in both pre and post-cracking regions.

The area under the curve and displacements also increased for the specimens prepared with steel fibre. For both Mix Designs A and B, the slope of the ascending branch of the curves was not significantly affected when using different fibre type and content; however, the descending branch for

specimens containing steel fibres showed significant improvement, demonstrating enhanced post-peak ductility and energy absorption capacity.

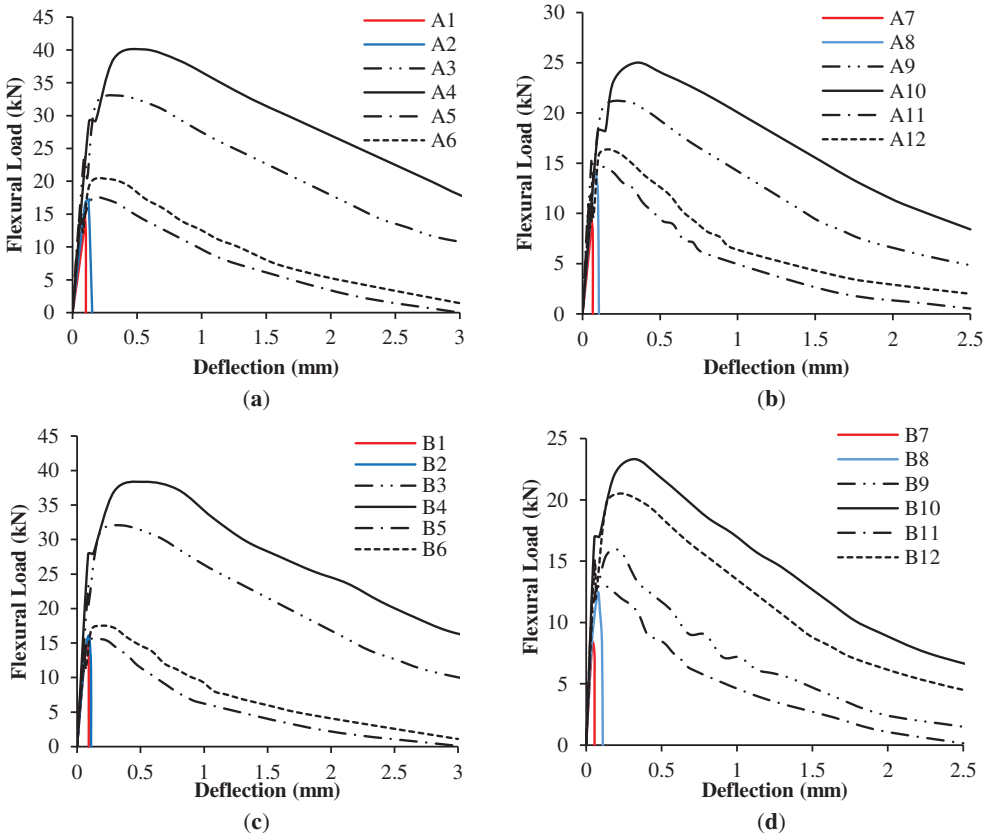

Figure 8: Load-deflection curves of UHPC mixes: (a) Mix A-microsilica, (b) Mix A-Class F fly ash, (c) Mix B-microsilica, and (d) Mix B-Class F fly ash

Figure 9: Flexural strength specimens of UHPC (a) steel (b) PP fibres

3.2.5 Drying Shrinkage

The influence of different types of SCMs, fibre type, and fibre content on the drying shrinkage (deformation due to air-drying) of UHPC specimens is shown in Fig. 10. It was observed that the drying shrinkage was increased rapidly till 14 days of air drying, which increased more slowly and remained nearly constant after 56 days for the case of specimens prepared with micro silica

(Fig. 10a,c) and after 70 days for the case of specimens prepared with fly ash (Fig. 10b,d). This behaviour may be due to an increase in the stiffness of the concrete matrix over time. As concrete ages, its microstructure densifies, and the material becomes stiffer. It was also observed that the specimens prepared with micro silica initially exhibited higher drying shrinkage, which could be primarily due to its high fineness, high pozzolanic property, and over 90% SiO_2 content, which accelerates the hydration and refines pore structure of concrete. This reaction with $Ca(OH)_2$ forms C-S-H gel, which may increase capillary tension in fine pores under drying conditions, leading to higher shrinkage at early ages [3,6].

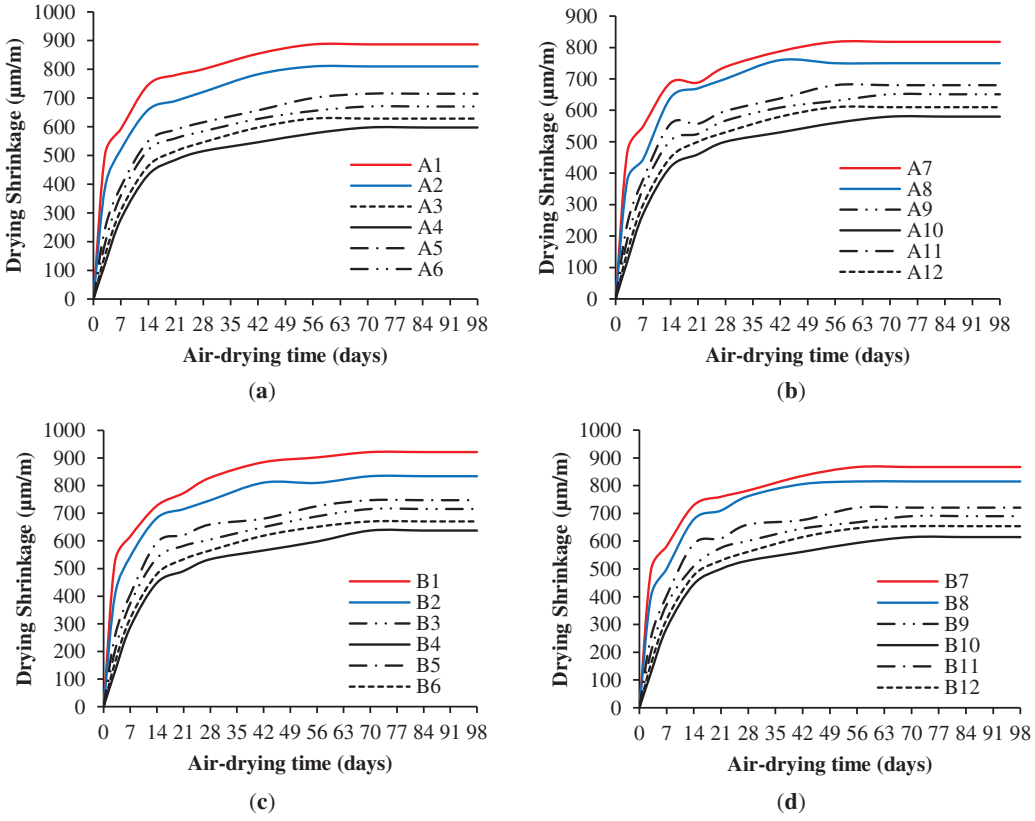

Figure 10: Drying shrinkage results of UHPC mixes: (a) Mix A-microsilica, (b) Mix A-Class F fly ash, (c) Mix B-microsilica, and (d) Mix B-Class F fly ash

The addition of fibres effectively restrained the deformation upon drying. Steel fibre-reinforced specimens showed less shrinkage than PP fibres and control specimens possibly due to their better ability to resist crack formation and improved crack bridging under tensile stresses. In contrast, PP fibres are better at reducing plastic shrinkage during early stages but provide limited long-term restraint due to their lower stiffness and tensile strength [22]. It should be noted that the 54 mm long PP fibres used in this study exceed the cross-section of the shrinkage prism (25 × 25 mm). Consequently, some fibre bending and preferential alignment along the prism length may occur, introducing potential wall effects. However, the high flexibility of PP fibres ensures bending occurs without breakage, and the influence on drying shrinkage is expected to be minor. Therefore, the results are interpreted comparatively, focusing on trends among mixes rather than absolute shrinkage values. Similar discussions have been reported in the previous studies [54–58].

The use of fly ash in UHPC specimens reduced the drying shrinkage at initial stages of hydration, which may be due to its relatively low reactivity delaying hydration and shrinkage development. As the curing process continues, its pozzolanic reaction could contributes to pore refinement, further reducing shrinkage. In addition, the specimens prepared with UFWGP were found to exhibit less shrinkage than the specimens without it. Silica in the glass powder may acts as a pozzolanic material, leading to the formation of additional C-S-H gel, which could help mitigate shrinkage in the binder matrix. The results found herein are consistent with previous findings [10,59].

4 Constitutive Modelling

The work presented here is the initial step towards the development of a global constitutive model for UHPC subjected to multiaxial states of stress. A uniaxial constitutive stress–strain model is formulated within the framework of elasto-damage mechanics by incorporating the effects of OPC, SCMs, w/b ratio, reinforcement index (RI), and fibre content (F) in UHPC, using the framework of elasto-damage mechanics for the uniaxial compression state of stress. The previously developed stress-strain model for concrete by Khan and Zahra [35] was considered as the basis and reformulated for UHPC.

To attain this objective, predictive equations for compressive strength ($f_c^{'}$) and Young's modulus (E_o) were first developed using both experimental data from this study and relevant data from existing literature. Initially, the model was evaluated using the β parameter proposed in the original Khan and Zahra model [35]. However, based on the stress-strain behaviour observed in the UHPC specimens, it was evident that the existing parameter β was not valid for predicting the stress-strain curves of UHPC. Therefore, a new equation for β was proposed, which provided significantly improved correlation with the experimental stress-strain curves of UHPC. A brief background of the original elasto-damage model for concrete, proposed by Khan and Zahra [35], is provided in this section, followed by the modified proposed model for UHPC

4.1 Elasto Damage Model for Concrete

The elasto-damage model of Khan and Zahra [35], proposed for predicting the behaviour of concrete under multi-axial loading conditions, uses continuum damage mechanics within the thermodynamic framework. The model is based on the associated flow rule and has restrictions in applying to different loading situations. Khan et al. [60] present a damage model that incorporates the theoretical aspects of this work. The key features of the model are as follows: fundamental surfaces are defined in the strain energy release space as given in Eqs. (3)–(5) (originally presented in Suaris et al. [61].

$$f = (R_i R_i)^{1/2} - \frac{R_c}{b} = 0 \tag{3}$$

$$F = (\overline{R}_i \overline{R}_i)^{1/2} - R_c = 0 \tag{4}$$

$$f_o = (R_i R_i)^{1/2} - R_0 = 0 \tag{5}$$

where, f is the loading function surface, F is the bounding surface, and f_o is a limit fracture surface.

The loading function surface f is defined in terms of thermodynamic-force conjugates, R_i in Eq. (6), where,

$$R_i = \rho \frac{\partial \Lambda}{\partial \omega_i} \left(\sigma_{ij}, \omega_i\right) \tag{6}$$

where ω_i, $i = 1, 2, 3$ are principal damage components. Also, $\partial\Lambda$ is the complementary energy density with ρ being the mass density. R_i is an image point on $F = 0$ associated with a given point R_i on $f = 0$ defined by a mapping rule Eqs. (7) and (8). A schematic view of these three surfaces used in the model is shown in Fig. 11.

$$\overline{R}_i = bR_i \tag{7}$$

$$b = R_c/\left(R_i R_i\right)^{1/2} \tag{8}$$

with the mapping parameter b ranging from an initial value of ∞ to a limiting value of 1 on growth of the loading surface to coalesce with the bounding surface. R_c, the critical strain energy release rate, is a parameter of the model that is calibrated to the standard uniaxial compression test. Damage is hypothesized to accumulate at levels of strain energy release rate, resulting in the loading surface f traversing the limit fracture surface f_o and rupture in the damage sense is said to occur when f grows large enough to coalesce with the bounding surface F fixed in the R_i space. For damaged materials, the constitutive equation may be expressed as in Eq. (9).

$$\epsilon = \frac{\partial\Lambda(\sigma,\omega)}{\partial\sigma} = \tilde{C}(E(\omega), \upsilon(\omega))\sigma \tag{9}$$

where $\tilde{C}$ is the effective compliance matrix for damaged material in the principal coordinate system and σ is the stress vector in the principal coordinate system. E is the elastic modulus and υ is the poisson's ratio. The complementary energy of a damaged material can be expressed as in Eq. (10).

$$\Lambda(\sigma,\omega) = \frac{1}{2}\sigma^T : \tilde{C} : \sigma \tag{10}$$

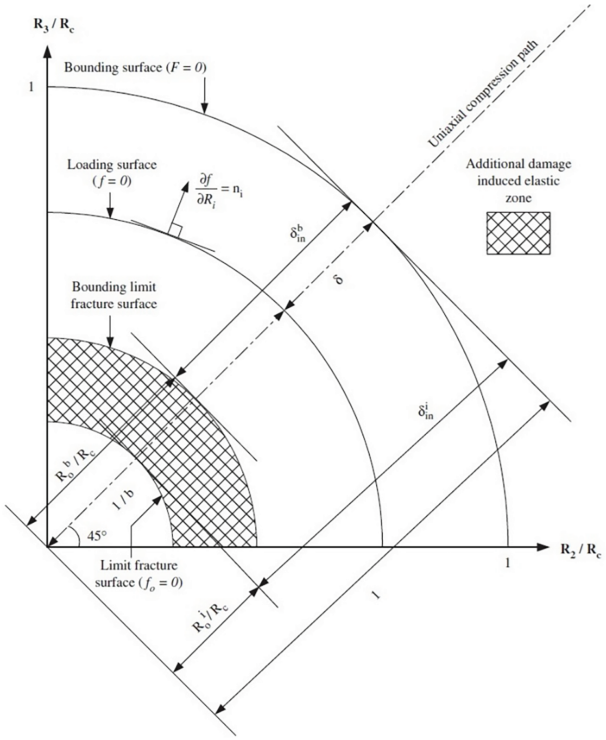

Figure 11: Limit fracture, loading and bounding surface (Khan and Zahra [35])

Based on physical insight and phenomenological evidence, the following elements of the compliance matrix $\tilde{C}$ are postulated in the principal coordinate system. The detailed formulation of $\tilde{C}$ is provided in [60]. In this framework, three calibrated material parameters, namely α,β, and γ, are introduced to reproduce the experimentally observed peak stress and volumetric dilatation behaviour of concrete, while E_o represents the initial elastic modulus. Parameter α governs the damage evolution under tensile stress states, β controls the damage growth under compressive stress states, and γ accounts for volumetric change associated with dilatancy. In addition, R_c is introduced as the critical strain energy release rate to regulate the overall damage growth rate in this model. The parameters α, β, and γ are represented as functions of the initial modulus of elasticity (E_o) and compressive strength ($f_c^{'}$) of the concrete in the uniaxial state and the strain invariants (I_1 & $J/_2$). Final forms of α, β, and γ for uniaxial compression are given in Eqs. (11)–(13). It is to be noted that they are unit sensitive, and "psi" should be used for $f_c^{'}$ and E_o in calculating these parameters.

$$\alpha = 0 \tag{11}$$

$$\beta = 0.643665 - 4.69309 \times 10^{-5} \times f_c^{'} - 7.71 \times 10^{-8} \times E_o + 6.022 \times 10^{-12} \times f_c^{/} \times E_o \tag{12}$$

$$\gamma = 3.1344 - 1.1826 \times 10^{-4} \times f_c^{'} - 2.903 \times 10^{-7} \times E_o + 1.28434 \times 10^{-11} \times f_c^{'} \times E_o \tag{13}$$

For the uniaxial state of compression, the constitutive model uses the strain-controlled incremental stress-strain relationship as given by Eq. (14). Details can be found elsewhere, (Khan et al. [60]).

$$d\sigma = \left(E_o \left(1 - \beta\omega\right)^4 - \frac{8\left(\beta^2 \varepsilon_1^2 E_o^2 \left(1 - \beta\omega\right)^6\right)}{\left(H + 3\left(\beta^2 \varepsilon_1^2 E_o \left(1 - \beta\omega\right)^2\right)\right)} \right) d\varepsilon_1 \tag{14}$$

where H is the damage modulus, which is expressed as a function of the distance between the loading and the bounding surface, and its value varies from ∞ to 0.

4.2 Proposed UHPC Elasto-Damage Model

As observed extensively in the published literature, UHPC mechanical properties such as compressive strength ($f_c^{'}$) and modulus of elasticity (E_o) are significantly influenced by mix constituents, including OPC, SCMs, w/b ratio, RI, and fibre content. Furthermore, the elasto-damage model proposed by Khan and Zahra [35] for predicting the behaviour of concrete incorporates the parameters α,β, and γ, which are functions of $f_c^{'}$ and E_o. Therefore, to consider the material-specific effects in the constitutive framework, empirical relationships for predicting $f_c^{'}$ and E_o were developed to use in the constitutive equations. Subsequently, the parameterβ for controlling the behaviour in compression was recalibrated through regression analysis using both experimental and published data as given in Appendices A and B.

4.2.1 Compressive Strength ($f_c^{'}$) Prediction of UHPC

The parameter "β", a compressive parameter controlling damage growth under compressive stress states, is expressed as a function of $f_c^{'}$ and E_o and varies according to the mix parameters. As discussed in preceding sections, the variables OPC, SCMs, w/b ratio, fibre content (F), and reinforcement index (RI) have a significant effect on the compressive strength of UHPC. All variables have a positive effect, except for the w/b ratio, as a substantial reduction in $f_c^{'}$ is observed with an increase in the w/b ratio. Therefore, to quantify these effects, experimental data from the present study, together with the literature data comprising 105 UHPC mixes with varying OPC, SCMs, w/b ratio, fibre content (F), and reinforcement index (RI) as given in Appendix A, were used to develop predictive equations

for $f_c^{'}$ using nonlinear least-squares fitting regression technique. The independent variables were OPC, SCMs (kg/m^3), w/b ratio, fibre content (F, kg/m^3), and reinforcement index (RI), and the dependent variable was the compressive strength ($f_c^{'}$). All the input variables were used in kg/m^3, while the output compressive strength $f_c^{'}$ was expressed in psi; therefore, the regression coefficients implicitly incorporate the unit conversion and scaling effects. The model is valid when the input parameters are used in the same units as adopted during model development. The proposed predictive equation for $f_c^{'}$ of UHPC is given in Eq. (15). The equation was validated against this combined dataset, showing high accuracy ($R^2 = 0.8815$), root mean square error (RMSE) = 10.1 MPa, and mean absolute error (MAE) = 7.4 MPa. Fig. 12 compares the predicted and experimental compressive strengths values for all the mixes provided in Appendix A. Iterative optimization minimized the difference between predicted and experimental compressive strengths.

$$f_c^{'}\,(psi) = 2146.56 + 162.44 \times \left(\frac{OPC + SCM}{\frac{w}{b}}\right)^{0.5} + 319.08 \times F^{0.4} + 899.24 \times RI + 8.70 \times F \times RI \quad (15)$$

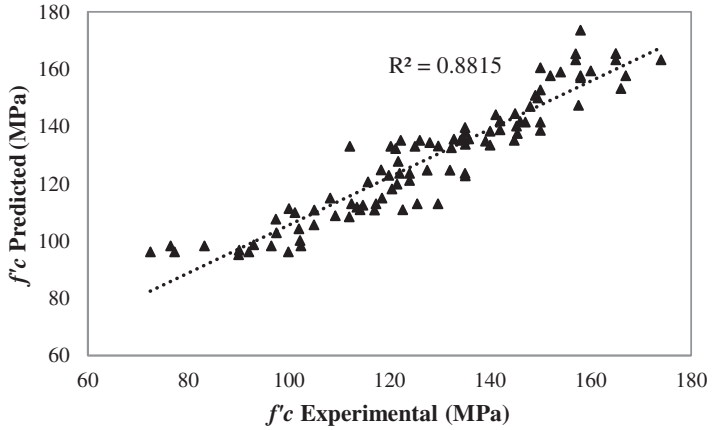

Figure 12: Comparison of experimental and predicted compressive strengths

4.2.2 Modulus of Elasticity (E_o) Prediction of UHPC

As discussed earlier, $f_c^{'}$ has a significant effect on the concrete MOE. An increase in $f_c^{'}$ results in a significant increase in MOE. Therefore, experimental data from this study and published literature were used, and nonlinear regression model was developed of UHPC, given by Eqs. (16) and (17). Fig. 13 shows the comparison between the predicted and experimental MOE of UHPC. The predicted MOE for all the mixes is provided in Appendix B.

$$E_c\,(MPa) = 3780\sqrt{f_c'} + 8000 \quad (16)$$

$$E_c\,(psi) = 548243.64\sqrt{f_c'} + 1160304 \quad (17)$$

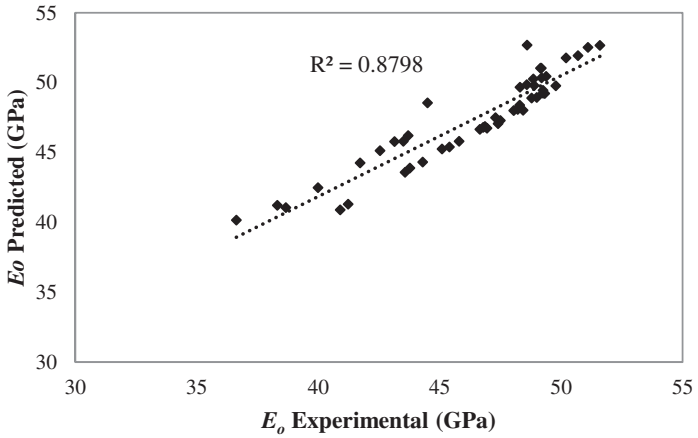

Figure 13: Comparison of predicted and experimental MOE

4.2.3 Compressive Parameter "β" Prediction for UHPC

The proposed parameter β for UHPC is defined as a function of compressive strength ($f_c^{'}$) and Young's modulus (E_o), reflecting the material's compressive stress-strain behaviour in Eq. (18).

$$\beta = 0.286573 - 2.1133034 \times 10^{-5} \times f_c^{'} - 2.834071 \times 10^{-8} \times E_o + 2.491057 \times 10^{-12} \times f_c^{'} \times E_o \quad (18)$$

4.3 Discussion on Stress-Strain Curves

EDUHPC (**E**lasto-**D**amage **M**odel for **U**ltra **H**igh **P**erformance **C**oncrete), a modified version of EDMON3D, a computer program developed by Khan and Zahra [35], is employed to predict the uniaxial stress strain behaviour of UHPC. Accordingly, the effects of fibres and SCMs on the elasto-damage constitutive model were evaluated by employing the experimentally obtained values of $f_c^{'}$ and E_o of the UHPC specimens in the model equations. A comparison between the experimental results and model predictions was then carried out. The experimental and predicted results of $f_c^{'}$ of this study are presented in Table 5, while the stress–strain curves of all the mixes of Mix Design A and Mix Design B are compared with the model in Figs. 14 and 15. The validation of model with existing literature was also carried out and is illustrated in Fig. 16.

The predicted stress-strain curves are presented in Figs. 14 and 15 and compared against the experimental results of this study and the previous model [35]. For validation, UHPC studies were considered, and the properties of concrete are summarized in Table 7. It was observed that the proposed model is predicting the stress-strain response better, particularly in capturing peak stresses, which has been attained as observed experimentally. In contrast, the previous model overestimated the compressive strength response. Furthermore, the predicted stress-strain curves correlate well with the experimental data, validating the robustness of the model.

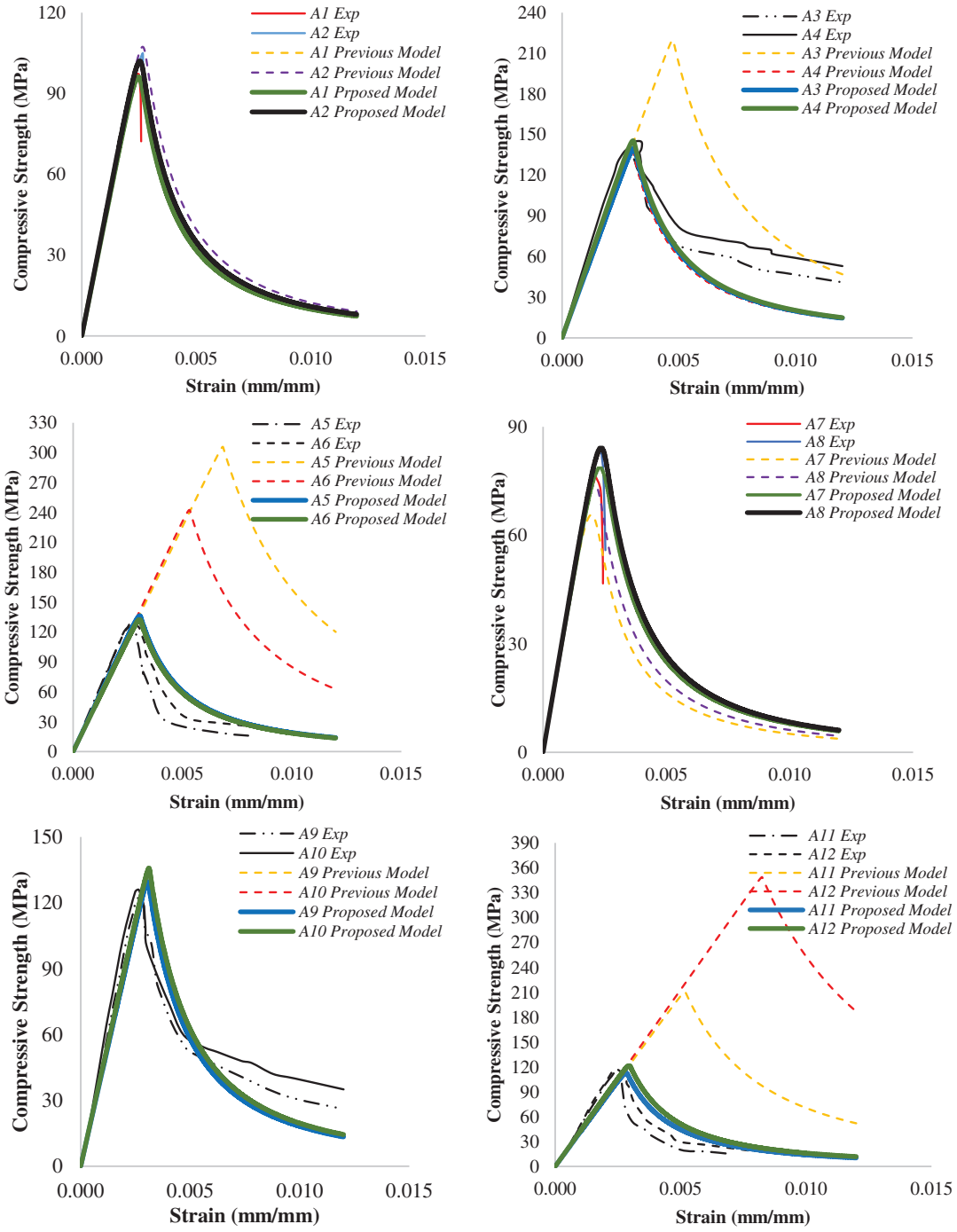

Figure 14: Predicted compressive strength test results of mix design A UHPC specimens

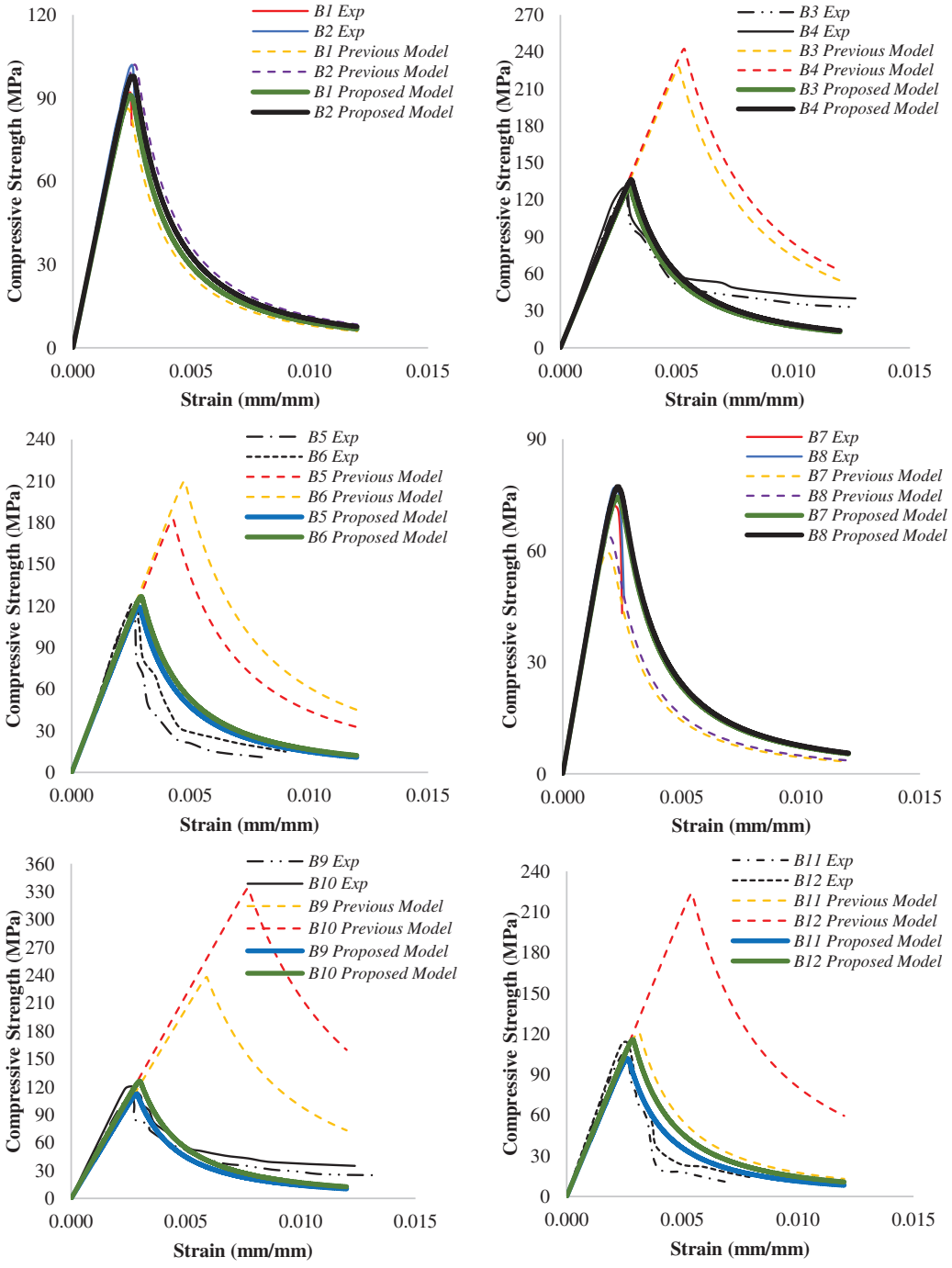

Figure 15: Predicted compressive strength test results of mix design B UHPC specimens

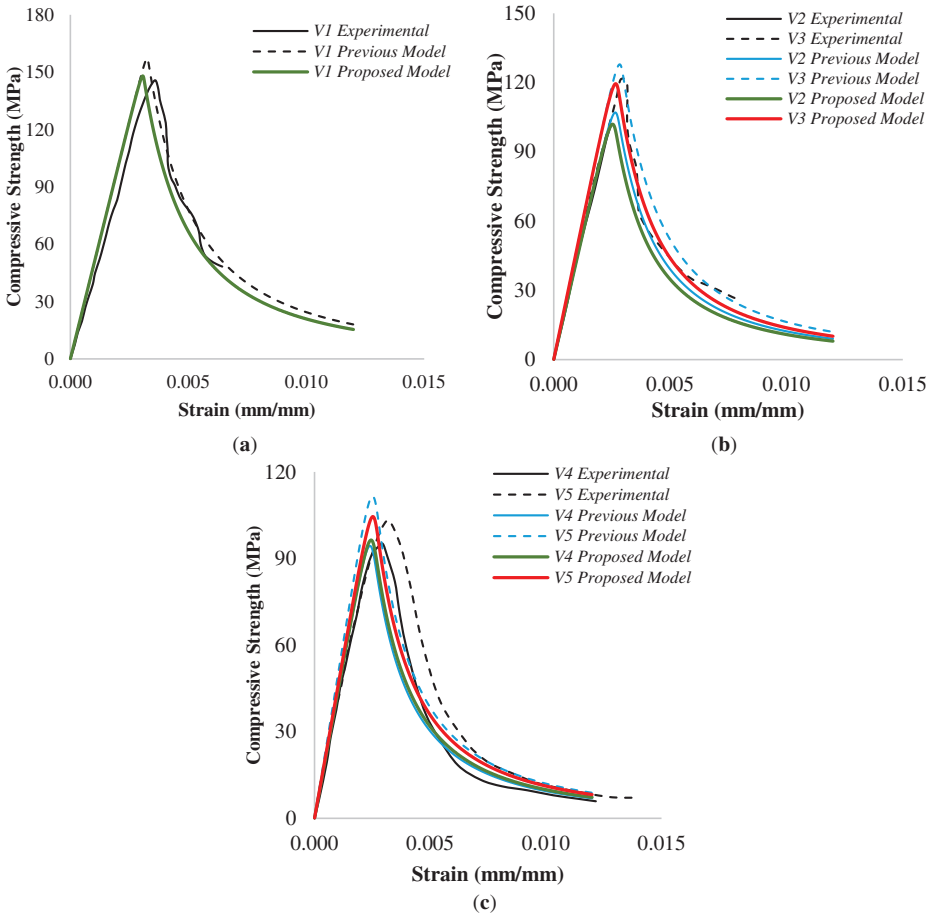

Figure 16: Validation of uniaxial compressive stress strain curves of concretes (a) Wang et al. [62] (b) Ren et al. [63] and (c) Tang et al. [64]

Table 7: Properties of UHPC used

Concrete	$f_c^{'}$ Experimental (MPa, psi)	E_o ($\times 10^6$ psi)	$f_c^{'}$ Predicted (MPa, psi)	*Relative residual* %
V1 (Wang et al. [62])	148.5, 21,538	7.208	148.2	0.20
V2 (Ren et al. [63])	102.2, 14,823	6.338	102.0	0.19
V3 (Ren et al. [63])	121.5, 17,622	7.005	119.3	1.81
V4 (Tang et al. [64])	95.1, 13,793	6.295	96.5	−1.47
V5 (Tang et al. [64])	111.5, 16,172	7.121	111.7	−0.17

The main difference arises in the post-peak response, where the model captures the softening behaviour of fibre reinforced specimens to a significant extent. This limitation is mainly due to the complex post-cracking behaviours involved in fibre bridging, pull-out, and debonding, which induce highly localized and discontinuous responses that are difficult to capture using continuum-based

frameworks. Also, it is experimentally difficult to measure the strains accurately in the post-peak softening regime due to crack localization, further complicating model validation.

The proposed model accurately predicts the stress–strain response up to peak compressive stress, closely matching experimental observations, whereas the previous model consistently overestimated peak strength. Despite these challenges, the proposed EDUHPC model proves to have a satisfactory ability to reproduce the key features of the UHPC behaviour, including peak strength and softening phase. This verifies its applicability as a reliable tool for modelling the performance of UHPC and establishes a foundation for future enhancements to include more detailed interactions between the fibre-matrix.

5 Conclusions

The following conclusions can be drawn based on the results from this study:

- Fresh and Hardened state properties of UHPC are strongly influenced by the combined effects of fibres, SCMs and following the optimized mixing procedures.
- Flowability of UHPC strongly depends on the type of fibres its geometry and SCMs used. Steel fibres significantly reduce the flowability due to increased interparticle friction as compared to crimped PP fibres. Fly ash enhances flowability by decreasing plastic viscosity, whereas micro silica increases density and cohesiveness, resulting in increased plastic viscosity and reduced flowability. Addition of UFWGP helps improve flowability due the spherical particles which reduces internal friction, acting as a lubricant between sand and fibres.
- The mechanical properties parameters including compressive, splitting tensile and flexural strengths, as well as the MOE are enhanced when steel fibres are combined with microsilica and UFWGP.
- Micro silica contributes to superior strength, mixes containing fly ash exhibit improved drying shrinkage resistance. The difference arises from the reaction kinetics: micro silica accelerates early hydration and increases shrinkage, whereas fly ash slows hydration, leading to reduced shrinkage at early ages.
- The proposed constitutive model is capable to predicts the stress-strain behaviour of UHPC with strong agreement to experimental results of this study and published data with prediction errors generally within $\pm 7\%$ of experimental results ranging from 72.4 to 148.5 MPa. Thus, providing a reliable framework for design and numerical simulation.
- Tailoring fibre types and SCM combinations is essential for optimizing strength, stiffness, flowability, and shrinkage, offering practical guidance for UHPC design in structural applications.

Acknowledgement: The authors would like to acknowledge the support provided by the Department of Civil Engineering at NED University of Engineering and Technology, Karachi, Pakistan in the pursuit of this work.

Funding Statement: The funding provided by the Higher Education Commission of Pakistan for the NRPU project no. 17069 titled “Impact behavior of Ultra High strength concrete RC structural members” and the funding provided by the MoST Endowment Fund committee under Office order No. Acad-628 II/50(48)/4886.

Author Contributions: The authors confirm contribution to the paper as follows: Conceptualization, Asad-ur-Rehman Khan and Shamsoon Fareed; methodology, Asad-ur-Rehman Khan and Shamsoon Fareed; software, Ayesha Ayub and Asad-ur-Rehman Khan; methodology; validation, Ayesha Ayub, Asad-ur-Rehman Khan and Shamsoon Fareed; formal analysis, Ayesha Ayub and Shamsoon Fareed; investigation, Ayesha Ayub, Asad-ur-Rehman Khan and Shamsoon Fareed; resources, Asad-ur-Rehman Khan and Shamsoon Fareed; data curation, Ayesha Ayub; writing—original draft preparation, Ayesha Ayub; writing—review and editing, Asad-ur-Rehman Khan and Shamsoon Fareed; visualization, Ayesha Ayub, Asad-ur-Rehman Khan and Shamsoon Fareed; supervision, Asad-ur-Rehman Khan and Shamsoon Fareed; project administration, Asad-ur-Rehman Khan and Shamsoon Fareed; funding acquisition, Ayesha Ayub and Shamsoon Fareed. All authors reviewed and approved the final version of the manuscript.

Availability of Data and Materials: The authors confirm that the data supporting the findings of this study are available within the article.

Ethics Approval: Not applicable.

Conflicts of Interest: The authors declare no conflicts of interest.

References

1. Kravanja G, Mumtaz AR, Kravanja S. A comprehensive review of the advances, manufacturing, properties, innovations, environmental impact and applications of ultra-high-performance concrete (UHPC). Buildings. 2024;14(2):382. doi:10.3390/buildings14020382.
2. Ocelić A, Baričević A, Smrkić MF. Synergistic integration of waste fibres and supplementary cementitious materials to enhance sustainability of ultra-high-performance concrete (UHPC). Case Stud Constr Mater. 2024;20(1):e02772. doi:10.1016/j.cscm.2023.e02772.
3. Lee NK, Koh KT, Kim MO, Ryu GS. Uncovering the role of micro silica in hydration of ultra-high performance concrete (UHPC). Cem Concr Res. 2018;104(12):68–79. doi:10.1016/j.cemconres.2017.11.002.
4. Shihada S, Arafa M. Effects of silica fume, ultrafine and mixing sequences on properties of ultra high performance concrete. Asian J Mater Sci. 2010;2(3):137–46. doi:10.3923/ajmskr.2010.137.146.
5. Wu Z, Shi C, Khayat KH. Influence of silica fume content on microstructure development and bond to steel fiber in ultra-high strength cement-based materials (UHSC). Cem Concr Compos. 2016;71(3):97–109. doi:10.1016/j.cemconcomp.2016.05.005.
6. Zheng Q, Li C, He B, Jiang Z. Revealing the effect of silica fume on the flexural behavior of ultra-high-performance fiber-reinforced concrete by acoustic emission technique. Cem Concr Compos. 2022;131(6):104563. doi:10.1016/j.cemconcomp.2022.104563.
7. Szcześniak A, Siwiński J, Stolarski A, Piekarczuk A, Nasiłowska B. The influence of the addition of microsilica and fly ash on the properties of ultra-high-performance concretes. Materials. 2025;18(1):28. doi:10.3390/ma18010028.
8. Jing R, Liu Y, Yan P. Uncovering the effect of fly ash cenospheres on the macroscopic properties and microstructure of ultra high-performance concrete (UHPC). Constr Build Mater. 2021;286(6):122977. doi:10.1016/j.conbuildmat.2021.122977.
9. Bahedh MA, Jaafar MS. Ultra high-performance concrete utilizing fly ash as cement replacement under autoclaving technique. Case Stud Constr Mater. 2018;9(4):e00202. doi:10.1016/j.cscm.2018.e00202.
10. Fu D, Xia C, Xu S, Zhang C, Jia X. Effect of concrete composition on drying shrinkage behavior of ultra-high performance concrete. J Build Eng. 2022;62(2):105333. doi:10.1016/j.jobe.2022.105333.

11. Van Tuan N, Dong PS, Thanh LT, Thang NC, Hyeok YK. Mix design of high-volume fly ash ultra high performance concrete. J Sci Technol Civ Eng STCE HUCE. 2021;15(4):197–208. doi:10.31814/stce.huce(nuce)2021-15(4)-17.
12. Soliman NA, Tagnit-Hamou A. Development of ultra-high-performance concrete using glass powder-towards ecofriendly concrete. Constr Build Mater. 2016;125(7):600–12. doi:10.1016/j.conbuildmat.2016.08.073.
13. Mohamed MAM, Elgabbas F, El-Nemr A, Khalaf MA. The influence of glass powder as a cement replacement material on ultra-high-performance concrete. CERM. 2021;43:315–23.
14. Taha B, Nounu G. Properties of concrete contains mixed colour waste recycled glass as sand and cement replacement. Constr Build Mater. 2008;22(5):713–20. doi:10.1016/j.conbuildmat.2007.01.019.
15. Sharifi Y, Afshoon I, Firoozjaei Z, Momeni A. Utilization of waste glass micro-particles in producing self-consolidating concrete mixtures. Int J Concr Struct Mater. 2016;10(3):337–53. doi:10.1007/s40069-016-0141-z.
16. Jalalinejad M, Hemmati A, Mortezaei A. Mechanical and durability properties of sustainable self-compacting concrete with waste glass powder and silica fume. Period Polytech Civil Eng. 2023;67:785–94. doi:10.3311/ppci.21537.
17. Prem PR, Bharatkumar B, Iyer NR. Mechanical properties of ultra high performance concrete. World Acad Sci Eng Technol. 2012;68:676–85. doi:10.5281/ZENODO.1327940.
18. Wu Z, Shi C, He W, Wu L. Effects of steel fiber content and shape on mechanical properties of ultra high performance concrete. Constr Build Mater. 2016;103(7):8–14. doi:10.1016/j.conbuildmat.2015.11.028.
19. Sharobim K, Hussien N. Mechanical properties of UHPC with hybrid fibers. Port Said Eng Res J. 2014;18(1):106–13. doi:10.21608/pserj.2014.46805.
20. Prem PR, Ramachandra Murthy A, Bharatkumar BH. Influence of curing regime and steel fibres on the mechanical properties of UHPC. Mag Concr Res. 2015;67(18):988–1002. doi:10.1680/macr.14.00333.
21. Le Hoang A, Fehling E. Influence of steel fiber content and aspect ratio on the uniaxial tensile and compressive behavior of ultra high performance concrete. Constr Build Mater. 2017;153(5):790–806. doi:10.1016/j.conbuildmat.2017.07.130.
22. Ahmad J, Burduhos-Nergis DD, Arbili MM, Alogla SM, Majdi A, Deifalla AF. A review on failure modes and cracking behaviors of polypropylene fibers reinforced concrete. Buildings. 2022;12(11):1951. doi:10.3390/buildings12111951.
23. Sounthararajan VM, Thirumurugan S, Sivakumar A. Reinforcing efficiency of crimped profile of polypropylene fibres on the cementitious matrix. Res J Appl Sci Eng Technol. 2013;6(14):2662–7. doi:10.19026/rjaset.6.3755.
24. He J, Chen W, Zhang B, Yu J, Liu H. The mechanical properties and damage evolution of UHPC reinforced with glass fibers and high-performance polypropylene fibers. Materials. 2021;14(9):2455. doi:10.3390/ma14092455.
25. Sohaib N, Mamoon R, Sana G, Seemab F. Using polypropylene fibers in concrete to achieve maximum strength. In: Proceedings of the Eighth International Conference on Advances in Civil and Structural Engineering—CSE 2018; 2018 Feb 4; Kuala Lumpur, Malaysia. doi:10.15224/978-1-63248-145-0-36.
26. Ramujee K. Strength properties of polypropylene fiber reinforced concrete. Int J Innov Res Sci Eng Technol. 2013;2:3409–13. doi:10.7324/ijerat.2018.3199.
27. Aly T, Sanjayan JG, Collins F. Effect of polypropylene fibers on shrinkage and cracking of concretes. Mater Struct. 2008;41(10):1741–53. doi:10.1617/s11527-008-9361-2.
28. Bouziadi F, Boulekbache B, Hamrat M. The effects of fibres on the shrinkage of high-strength concrete under various curing temperatures. Constr Build Mater. 2016;114(2):40–8. doi:10.1016/j.conbuildmat.2016.03.164.
29. Guo Z. Principles of reinforced concrete. Oxford, UK: Butterworth-Heinemann; 2014.

30. Saenz L, Discussion of paper by Desai P, Krishnan S. Equation for stress-strain curve of concrete. J ACI Proc. 1964;61(3):61.
31. Xiao S, Yang J, Liu Z, Yang W, He J. Effects of steel fiber content on compressive properties and constitutive relation of ultra-high performance shotcrete (UHPSC). Buildings. 2024;14(6):1503. doi:10.3390/buildings14061503.
32. Jiao CJ, Sun W, Qin HG, Zhang YM, Jiang JY. Uniaxial compression constitutive equation of steel-fiber high-strength concrete. J Southeast Univ (Nat Sci Ed). 2004;34:366–9. (In Chinese).
33. Ju YZ, Wang DH, Li QC, Jia YZ, Xiao Q. Effect of steel fiber content on mechanical properties of reactive powder concrete. J Exp Mech. 2011;26:254–60. (In Chinese).
34. Al-Hassani HM, Khalil WI, Danha LS. Proposed model for uniaxial compression behavior of reactive powder concrete. J Babylon Univ Eng Sci. 2015;23(3):591–606. doi:10.30684/etj.33.1a.5.
35. Khan AR, Zahra T. Elasto-damage modeling of concrete subjected to proportionate and non-proportionate multiaxial state of stress. J Mech Continua Math Sci. 2019;14(2):7–26. doi:10.26782/jmcms.2019.04.00002.
36. American Concrete Institute. ACI 239R-18: ultra-high-performance concrete: an emerging technology report. Farmington Hills, MI, USA: American Concrete Institute; 2018.
37. AQUAFIN. Remicrete PCSP super plasticizer. [cited 2025 Apr 8]. Available from: https://www.aquafinpakistan.com/products/tds-remicrete-pcsp/.
38. Abdulghani MR, Ali DAS. Flexural behavior of reinforced concrete beams reinforced with 3D-textile composite fiber. J Eng. 2020;26(7):127–44. doi:10.31026/j.eng.2020.07.09.
39. Anhui Elite Industrial Co., Ltd. Polypropylene (PP) fiber crimped. [cited 2025 Apr 8]. Available from: https://www.ahelite.com/Polypropylene-PP-Fiber-wave-curved-pd479524.html.
40. Du J, Meng W, Khayat KH, Bao Y, Guo P, Lyu Z, et al. New development of ultra-high-performance concrete (UHPC). Compos Part B Eng. 2021;224(9):109220. doi:10.1016/j.compositesb.2021.109220.
41. Meng W, Valipour M, Khayat KH. Optimization and performance of cost-effective ultra-high performance concrete. Mater Struct. 2016;50(1):29. doi:10.1617/s11527-016-0896-3.
42. ASTM International. ASTM C1437-20: standard test method for flow of hydraulic cement mortar. West Conshohocken, PA, USA: ASTM International; 2020. p. 1–2. doi:10.1520/C1437-20.
43. ASTM International. ASTM D2196-18: standard test methods for rheological properties of non-newtonian materials by rotational viscometer. West Conshohocken, PA, USA: ASTM International; 2018. p. 1–5. doi:10.1520/D2196-1810.1520/D2196-18.
44. ASTM International. ASTM C39/C39M-20: standard test method for compressive strength of cylindrical concrete specimens. West Conshohocken, PA, USA: ASTM International; 2018. p. 1–8. doi:10.1520/C0039_C0039M-20.
45. ASTM International. ASTM C469/C469M-14: standard test method for static modulus of elasticity and Poisson's ratio of concrete in compression. West Conshohocken, PA, USA: ASTM International; 2014. p. 1–5. doi:10.1520/C0469_C0469M-14.
46. ASTM International. ASTM C496/C496M-17: standard test method for splitting tensile strength of cylindrical concrete specimens. West Conshohocken, PA, USA: ASTM International; 2017. p. 1–5. doi:10.1520/C0496_C0496M-17.
47. ASTM International. ASTM C78/C78M-10: standard test method for flexural strength of concrete (using simple beam with third-point loading). West Conshohocken, PA, USA: ASTM International; 2010. p. 1–4. doi:10.1520/C0078_C0078M-10.
48. ASTM International. ASTM C157/C157M-17a: standard test method for length change of hardened hydraulic-cement mortar and concrete. West Conshohocken, PA, USA: ASTM International; 2017. p. 1–8. doi:10.1520/C0157_C0157M-17.

49. Bazhuni MF, Kamali M, Ghahremaninezhad A. An investigation into the properties of ternary and binary cement pastes containing glass powder. Front Struct Civ Eng. 2019;13(3):741–50. doi:10.1007/s11709-018-0511-5.
50. Galobardes I, Cavalaro SH, Aguado A, Garcia T. Estimation of the modulus of elasticity for sprayed concrete. Constr Build Mater. 2014;53(1):48–58. doi:10.1016/j.conbuildmat.2013.11.046.
51. Kusumawardaningsih Y, Fehling E, Ismail M, Aboubakr AAM. Tensile strength behavior of UHPC and UHPFRC. Procedia Eng. 2015;125:1081–6. doi:10.1016/j.proeng.2015.11.166.
52. Yoo DY, Shin HO, Yang JM, Yoon YS. Material and bond properties of ultra high performance fiber reinforced concrete with micro steel fibers. Compos Part B Eng. 2014;58(3):122–33. doi:10.1016/j.compositesb.2013.10.081.
53. Du W, Yu F, Qiu L, Guo Y, Wang J, Han B. Effect of steel fibers on tensile properties of ultra-high-performance concrete: a review. Materials. 2024;17(5):1108. doi:10.3390/ma17051108.
54. Shen D, Liu X, Zeng X, Zhao X, Jiang G. Effect of polypropylene plastic fibers length on cracking resistance of high performance concrete at early age. Constr Build Mater. 2020;244(5):117874. doi:10.1016/j.conbuildmat.2019.117874.
55. Almeida Del Savio A, La Torre Esquivel D, García Landeo JM. Post-cracking properties of concrete reinforced with polypropylene fibers through the Barcelona test. Polymers. 2023;15(18):3718. doi:10.3390/polym15183718.
56. Arslan KM, Karagüler ME. Shrinkage cracking and mechanical properties of cementitious composites produced with multiwall carbon nano tubes and different types of polypropylene fibres. Constr Build Mater. 2024;420:135599. doi:10.1016/j.conbuildmat.2024.135599.
57. Bentur A, Mindess S. Fibre reinforced cementitious composites. Boca Raton, FL, USA: CRC Press; 2006.
58. Li M, Li VC. Rheology, fiber dispersion, and robust properties of engineered cementitious composites. Mater Struct. 2013;46(3):405–20. doi:10.1617/s11527-012-9909-z.
59. Ibrahim MAFM, Issa MA, Hasse JA. Effect of material constituents on mechanical and fracture mechanics properties of ultra-high-performance concrete. ACI Mater J. 2017;114(3):453–65. doi:10.14359/51689717.
60. Khan AR, Al-Gadhib AH, Baluch MH. Elasto-damage model for high strength concrete subjected to multiaxial loading. Int J Damage Mech. 2007;16(3):361–98. doi:10.1177/1056789506065914.
61. Suaris W, Ouyang C, Fernando VM. Damage model for cyclic loading of concrete. J Eng Mech. 1990;116(5):1020–35. doi:10.1061/(asce)0733-9399(1990)116:.
62. Wang YZ, Wang YB, Zhao YZ, Li GQ, Lyu YF, Li H. Experimental study on ultra-high performance concrete under triaxial compression. Constr Build Mater. 2020;263(3):120225. doi:10.1016/j.conbuildmat.2020.120225.
63. Ren GM, Wu H, Fang Q, Liu JZ. Effects of steel fiber content and type on static mechanical properties of UHPCC. Constr Build Mater. 2018;163(6):826–39. doi:10.1016/j.conbuildmat.2017.12.184.
64. Tang X, He B, Yang B, Chen J. Experimental study on axial stress-strain behaviour of steel fibre-reinforced steel slag micropowder UHPC. Appl Sci. 2023;13(15):8807. doi:10.3390/app13158807.
65. Tayeh BA, Akeed MH, Qaidi S, Abu Bakar BH. Ultra-high-performance concrete: impacts of steel fibre shape and content on flowability, compressive strength and modulus of rupture. Case Stud Constr Mater. 2022;17(1):e01615. doi:10.1016/j.cscm.2022.e01615.
66. Zhang SS, Wang JJ, Lin G, Yu T, Fernando D. Stress-strain models for ultra-high performance concrete (UHPC) and ultra-high performance fiber-reinforced concrete (UHPFRC) under triaxial compression. Constr Build Mater. 2023;370(9):130658. doi:10.1016/j.conbuildmat.2023.130658.
67. Wu Z, Shi C, He W, Wang D. Static and dynamic compressive properties of ultra-high performance concrete (UHPC) with hybrid steel fiber reinforcements. Cem Concr Compos. 2017;79(3):148–57. doi:10.1016/j.cemconcomp.2017.02.010.

68. Chen HJ, Yu YL, Tang CW. Mechanical properties of ultra-high performance concrete before and after exposure to high temperatures. Materials. 2020;13(3):770. doi:10.3390/ma13030770.
69. Choi D, Hong K, Ochirbud M, Meiramov D, Sukontaskuul P. Mechanical properties of ultra-high performance concrete (UHPC) and ultra-high performance fiber-reinforced concrete (UHPFRC) with recycled sand. Int J Concr Struct Mater. 2023;17(1):67. doi:10.1186/s40069-023-00631-2.
70. Wu Z, Shi C, Khayat KH. Investigation of mechanical properties and shrinkage of ultra-high performance concrete: influence of steel fiber content and shape. Compos Part B Eng. 2019;174(9):107021. doi:10.1016/j.compositesb.2019.107021.
71. Roberti F, Cesari VF, de Matos PR, Pelisser F, Pilar R. High- and ultra-high-performance concrete produced with sulfate-resisting cement and steel microfiber: autogenous shrinkage, fresh-state, mechanical properties and microstructure characterization. Constr Build Mater. 2021;268:121092. doi:10.1016/j.conbuildmat.2020.121092.
72. Fang H, Gu M, Zhang S, Jiang H, Fang Z, Hu J. Effects of steel fiber and specimen geometric dimensions on the mechanical properties of ultra-high-performance concrete. Materials. 2022;15(9):3027. doi:10.3390/ma15093027.
73. Nguyen TT, Thai HT, Ngo T. Effect of steel fibers on the performance of an economical ultra-high strength concrete. Struct Concr. 2023;24(2):2327–41. doi:10.1002/suco.202200326.
74. Abbas S, Soliman AM, Nehdi ML. Exploring mechanical and durability properties of ultra-high performance concrete incorporating various steel fiber lengths and dosages. Constr Build Mater. 2015;75(5):429–41. doi:10.1016/j.conbuildmat.2014.11.017.
75. Yin H, Shirai K, Teo W. Finite element modelling to predict the flexural behaviour of ultra-high performance concrete members. Eng Struct. 2019;183(7):741–55. doi:10.1016/j.engstruct.2019.01.046.
76. Al-Osta MA, Sharif AM, Ahmad S, Adekunle SK, Al-Huri M, Sharif AM. Effect of hybridization of straight and hooked steel fibers and curing methods on the key mechanical properties of UHPC. J Mater Res Technol. 2021;15(9):3222–39. doi:10.1016/j.jmrt.2021.10.005.
77. Yan X, Gao Y, Luo Y, Bi Y, Xie Y. Effect of different steel fiber types on mechanical properties of ultra-high performance concrete. IOP Conf Ser Mater Sci Eng. 2021;1167(1):12001. doi:10.1088/1757-899X/1167/1/012001.
78. Smarzewski P. Effect of curing period on properties of steel and polypropylene fibre reinforced ultra-high performance concrete. IOP Conf Ser Mater Sci Eng. 2017;245(3):32059. doi:10.1088/1757-899X/245/3/032059.
79. Qadir HH, Faraj RH, Sherwani AFH, Mohammed BH, Younis KH. Mechanical properties and fracture parameters of ultra high performance steel fiber reinforced concrete composites made with extremely low water per binder ratios. SN Appl Sci. 2020;2(9):1594. doi:10.1007/s42452-020-03425-3.
80. Meng W, Khayat KH. Effect of hybrid fibers on fresh properties, mechanical properties, and autogenous shrinkage of cost-effective UHPC. J Mater Civ Eng. 2018;30(4):4018030. doi:10.1061/(asce)mt.1943-5533.0002212.

Appendix A

Table A1: Properties of UHPC used

Authors	w/b	OPC	SCM	F	RI	f'_c Exp	f'_c Pre
		(kg/m^3)				(MPa)	
Tayeh et al. [65]	0.157	811.000	1092.000	69.000	0.325	122.000	123.655

(Continued)

Table A1 (continued)

Authors	w/b	OPC	SCM	F	RI	f'_c Exp	f'_c Pre
		(kg/m^3)				(MPa)	
	0.157	802.000	1078.000	148.000	0.975	150.000	138.615
	0.158	792.000	1057.000	226.000	1.625	158.000	157.752
	0.157	811.000	1092.000	69.000	0.325	124.000	123.655
	0.158	792.000	1057.000	226.000	1.625	167.000	157.752
	0.157	811.000	1092.000	69.000	0.325	135.000	123.655
	0.158	792.000	1057.000	226.000	1.625	170.000	157.752
He et al. [24]	0.173	750.000	1103.000	4.550	0.261	101.200	109.909
	0.173	750.000	1103.000	18.200	0.522	108.200	115.014
Zhang et al. [66]	0.208	800.000	1152.000	156.000	1.300	139.100	134.896
Wu et al. [67]	0.170	472.200	1049.000	0.000	0.000	97.500	102.861
	0.170	472.200	1049.000	156.000	1.300	135.000	139.672
Chen et al. [68]	0.195	1005.000	1005.000	0.000	0.000	90.000	95.200
Choi et al. [69]	0.200	891.000	1071.300	0.000	0.000	90.100	96.820
	0.160	931.000	1119.000	0.000	0.000	112.000	108.475
	0.170	832.000	1084.100	0.000	0.000	102.000	104.311
	0.160	842.000	1096.900	0.000	0.000	97.400	107.668
	0.170	832.000	1084.100	156.000	0.867	128.000	134.380
Prem et al. [17]	0.176	788.000	985.000	0.000	0.000	93.000	98.675
Sharobim et al. [19]	0.160	950.000	1187.500	0.000	0.000	100.000	111.288
Wu et al. [70]	0.180	863.000	1079.000	78.000	0.650	124.000	121.154
	0.180	863.000	1079.000	156.000	1.300	140.000	138.326
	0.180	863.000	1079.000	234.000	1.950	150.000	160.486
Roberti et al. [71]	0.200	970.000	970.000	59.700	0.488	109.200	108.861
	0.200	970.000	970.000	119.300	0.975	115.700	120.719
Ren et al. [63]	0.162	700.000	940.000	0.000	0.000	102.200	100.193
	0.162	700.000	940.000	39.000	0.325	114.700	112.493
	0.162	700.000	940.000	78.000	0.650	121.500	119.833
	0.162	700.000	940.000	117.000	0.975	121.700	127.864
	0.162	700.000	940.000	39.000	0.250	113.500	111.853
	0.162	700.000	940.000	78.000	0.500	120.500	118.201
	0.162	700.000	940.000	117.000	0.750	118.300	124.889
	0.162	700.000	940.000	156.000	1.000	121.200	132.337
Wu et al. [18]	0.164	809.000	1079.000	0.000	0.000	105.000	105.635
	0.164	800.000	1067.000	78.000	0.650	127.500	124.776
	0.164	792.000	1056.000	156.000	1.300	147.000	141.532
	0.164	784.000	1045.000	234.000	1.950	157.000	163.274
	0.164	800.000	1067.000	78.000	0.650	132.000	124.776
	0.164	792.000	1056.000	156.000	1.300	150.000	141.532
	0.164	784.000	1045.000	234.000	1.950	165.000	163.274

(Continued)

Table A1 (continued)

Authors	w/b	OPC	SCM	F	RI	f'_c Exp	f'_c Pre
		(kg/m^3)				(MPa)	
	0.164	784.000	1045.000	234.000	1.950	174.000	163.274
Fang et al. [72]	0.186	829.000	1045.000	156.000	1.182	135.070	133.802
	0.186	829.000	1045.000	234.000	1.773	138.450	154.213
	0.186	829.000	1045.000	156.000	1.455	135.090	138.047
	0.186	829.000	1045.000	156.000	1.280	134.860	135.330
	0.186	829.000	1045.000	156.000	1.300	135.740	135.641
Nguyen et al. [73]	0.145	800.000	1000.000	117.000	0.750	132.300	132.571
	0.145	800.000	1000.000	117.000	0.975	132.800	135.545
	0.145	800.000	1000.000	117.000	1.620	141.100	144.072
	0.145	800.000	1000.000	117.000	1.125	145.400	137.528
	0.145	800.000	1000.000	39.000	0.625	135.100	122.737
	0.145	800.000	1000.000	117.000	1.875	157.600	147.443
Abbas et al. [74]	0.184	800.000	1000.000	468.000	2.400	171.000	205.374
	0.184	800.000	1000.000	234.000	1.800	166.000	153.303
	0.184	800.000	1000.000	234.000	2.400	165.000	165.447
Yin et al. [75]	0.160	800.000	1000.000	78.000	0.650	119.830	122.984
	0.160	800.000	1000.000	156.000	1.300	145.270	140.155
Al-Osta et al. [76]	0.146	900.000	1120.000	157.000	1.300	149.500	149.984
Yan et al. [77]	0.180	790.000	1053.000	0.000	0.000	112.000	100.464
	0.180	790.000	1053.000	156.000	1.300	150.000	137.275
	0.180	790.000	1053.000	234.000	1.950	160.000	159.435
	0.180	790.000	1053.000	312.000	2.600	163.000	187.137
	0.180	790.000	1053.000	156.000	1.600	142.000	141.943
Smarzewski et al. [78]	0.239	670.500	745.000	9.000	4.800	118.500	114.991
	0.239	670.500	745.000	13.500	7.200	115.800	134.044
Qadir et al. [79]	0.120	998.800	1175.050	71.700	0.375	146.000	141.722
	0.120	998.800	1175.050	107.550	0.563	148.000	147.040
	0.120	998.800	1175.050	143.400	0.750	150.000	152.769
	0.120	998.800	1175.050	179.250	0.938	154.000	159.058
	0.120	998.800	1175.050	215.100	1.125	155.000	165.983
	0.120	998.800	1175.050	250.950	1.313	158.000	173.588
	0.120	998.800	1175.050	286.800	1.500	162.000	181.901
	0.140	998.800	1175.050	71.700	0.375	140.000	133.500
	0.140	998.800	1175.050	107.550	0.563	142.000	138.819
	0.140	998.800	1175.050	143.400	0.750	145.000	144.547
	0.140	998.800	1175.050	179.250	0.938	149.000	150.837
	0.140	998.800	1175.050	215.100	1.125	152.000	157.762
	0.140	998.800	1175.050	250.950	1.313	157.000	165.367
	0.140	998.800	1175.050	286.800	1.500	160.000	173.679

(Continued)

Table A1 (continued)

Authors	w/b	OPC	SCM	F	RI	f'_c Exp	f'_c Pre
		(kg/m^3)				(MPa)	
Meng et al. [80]	0.200	654.000	1104.700	234.000	1.950	158.000	157.010
	0.200	648.000	1094.300	312.000	2.600	150.000	184.320
Present	0.200	800.000	1111.200	0.000	0.000	96.510	98.291
Study	0.200	640.000	1111.200	0.000	0.000	102.350	98.291
	0.200	800.000	1111.200	157.000	1.300	134.090	135.223
	0.200	640.000	1111.200	157.000	1.300	144.780	135.223
	0.200	800.000	1111.200	13.700	1.200	125.500	112.985
	0.200	640.000	1111.200	13.700	1.200	129.660	112.985
	0.200	800.000	1111.200	0.000	0.000	76.440	98.291
	0.200	640.000	1111.200	0.000	0.000	83.190	98.291
	0.200	800.000	1111.200	157.000	1.300	122.220	135.223
	0.200	640.000	1111.200	157.000	1.300	126.050	135.223
	0.200	800.000	1111.200	13.700	1.200	112.420	112.985
	0.200	640.000	1111.200	13.700	1.200	117.310	112.985
	0.200	792.000	1056.000	0.000	0.000	92.010	96.183
	0.200	634.000	1056.400	0.000	0.000	99.860	96.214
	0.200	792.000	1056.000	157.000	1.300	125.050	133.115
	0.200	634.000	1056.400	157.000	1.300	129.680	133.146
	0.200	792.000	1056.000	13.700	1.200	117.010	110.877
	0.200	634.000	1056.400	13.700	1.200	122.600	110.908
	0.200	792.000	1056.000	0.000	0.000	72.420	96.183
	0.200	634.000	1056.400	0.000	0.000	77.240	96.195
	0.200	792.000	1056.000	157.000	1.300	112.090	133.115
	0.200	634.000	1056.400	157.000	1.300	120.270	133.127
	0.200	792.000	1056.000	13.700	1.200	105.020	110.877
	0.200	634.000	1056.400	13.700	1.200	114.120	110.889

Appendix B

Table A2: Properties of UHPC used

Authors	w/b	OPC	SCM	F	RI	f'_c	E_o Exp	E_o Pre
		(kg/m^3)		(MPa)			(GPa)	
He et al. [24]	0.173	750.000	1103.000	12.700	0.650	115.100	44.500	48.554
	0.173	750.000	1103.000	50.800	1.300	131.700	45.800	51.380
	0.173	750.000	1103.000	13.650	0.975	95.100	40.900	44.862
	0.173	750.000	1103.000	18.200	1.300	108.200	44.300	47.319

(Continued)

Table A2 (continued)

Authors	w/b	OPC	SCM	F	RI	f'_c	E_o Exp	E_o Pre
		(kg/m^3)		(MPa)			(GPa)	
Zhang et al. [66]	0.208	800.000	1152.000	0.000	0.000	113.400	45.100	48.253
Choi et al. [69]	0.200	891.000	1071.300	0.000	0.000	90.100	43.773	43.880
	0.160	931.000	1119.000	0.000	0.000	112.000	48.043	48.004
	0.160	842.000	1096.900	0.000	0.000	97.400	41.231	45.305
	0.170	832.000	1084.100	78.000	0.650	100.000	43.506	45.800
	0.170	832.000	1084.100	156.000	1.300	128.000	46.867	50.766
	0.170	832.000	1084.100	234.000	1.950	113.000	46.656	48.182
	0.160	842.000	1096.900	156.000	1.300	108.000	47.502	47.283
Roberti et al. [71]	0.200	970.000	970.000	0.000	0.000	106.800	47.400	47.064
	0.200	970.000	970.000	59.700	0.488	109.200	47.300	47.501
	0.200	970.000	970.000	119.300	0.975	115.700	46.800	48.659
Ren et al. [63]	0.162	700.000	940.000	0.000	0.000	102.200	43.700	46.214
	0.162	700.000	940.000	39.000	0.325	114.700	45.400	48.483
	0.162	700.000	940.000	78.000	0.650	121.500	48.300	49.666
Al-Osta et al. [76]	0.146	900.000	1120.000	157.000	1.300	149.500	49.330	54.218
Smarzewski et al. [78]	0.239	670.500	745.000	0.000	0.000	139.800	48.600	52.694
	0.239	670.500	745.000	4.500	0.325	134.100	50.200	51.773
	0.239	670.500	745.000	78.000	0.650	135.100	50.700	51.936
	0.239	670.500	745.000	117.000	0.975	138.700	51.100	52.517
	0.239	670.500	745.000	156.000	1.300	139.600	51.600	52.662
Present study	0.200	800.000	1111.200	0.000	0.000	96.510	42.540	45.135
	0.200	640.000	1111.200	0.000	0.000	102.350	43.580	46.242
	0.200	800.000	1111.200	157.000	1.300	134.090	49.250	51.771
	0.200	640.000	1111.200	157.000	1.300	144.780	49.780	53.483
	0.200	800.000	1111.200	13.700	0.975	125.500	49.200	50.346
	0.200	640.000	1111.200	13.700	0.975	129.660	49.180	51.042
	0.200	800.000	1111.200	0.000	0.000	76.440	38.670	41.049
	0.200	640.000	1111.200	0.000	0.000	83.190	39.990	42.477
	0.200	800.000	1111.200	157.000	1.300	122.220	48.890	49.789
	0.200	640.000	1111.200	157.000	1.300	126.050	49.380	50.439
	0.200	800.000	1111.200	13.700	0.975	112.420	48.210	48.079
	0.200	640.000	1111.200	13.700	0.975	117.310	49.000	48.941
	0.200	792.000	1056.000	0.000	0.000	92.010	41.720	44.258
	0.200	634.000	1056.400	0.000	0.000	99.860	43.140	45.774
	0.200	792.000	1056.000	157.000	1.300	125.050	48.860	50.270
	0.200	634.000	1056.400	157.000	1.300	129.680	49.150	51.046
	0.200	792.000	1056.000	13.700	0.975	117.010	48.790	48.889
	0.200	634.000	1056.400	13.700	0.975	122.600	48.590	49.854
	0.200	792.000	1056.000	0.000	0.000	72.420	36.630	40.168

(Continued)

Table A2 (continued)

Authors	w/b	OPC	SCM	F	RI	f'_c	E_o Exp	E_o Pre
		(kg/m^3)		(MPa)			(GPa)	
	0.200	634.000	1056.400	0.000	0.000	77.240	38.320	41.221
	0.200	792.000	1056.000	157.000	1.300	112.090	48.440	48.020
	0.200	634.000	1056.400	157.000	1.300	120.270	49.250	49.454
	0.200	792.000	1056.000	13.700	0.975	105.020	46.950	46.737
	0.200	634.000	1056.400	13.700	0.975	114.120	48.290	48.381